Full length article

# Fire design of steel columns through second-order inelastic analysis with strain limits

Hasan Murtaza, Merih Kucukler *

*School of Engineering, University of Warwick, Coventry, CV4 7AL, UK*

## ARTICLE INFO

## ABSTRACT

A structural steel fire design approach through second-order inelastic analysis with strain limits is proposed and applied to the fire design of steel columns as a first step in the establishment of a novel fire design framework for steel structures in this paper. The proposed method is carried out using beam finite elements, utilising their computational efficiency. In the proposed design approach, the strength and stiffness deterioration of steel in fire, the spread of plasticity, global instability effects, indirect fire actions and thermal expansion are fully taken into account through second-order inelastic analysis, while strain limits are employed to consider the deleterious influence of local buckling on the ultimate resistance. Ultimate capacity of a steel member or system is determined by (i) the load or temperature level at which the predefined strain limit is attained or (ii) the peak load or critical temperature observed during the analysis, whichever occurs first. A systematic numerical parametric study is carried out through nonlinear shell finite element modelling, taking into account a high number of I-section and hollow section steel columns whose response is considered (i) using isothermal and anisothermal analysis techniques and (ii) with and without axial and rotational end-restraints. It is demonstrated that the proposed fire design approach consistently furnishes significantly more accurate capacity and limit temperature predictions for steel columns in fire relative to EN 1993-1-2 [1] design provisions.

## 1. Introduction

Fire design of steel structures presents a significant challenge to structural engineers due to the complexity of structural response in fire and the major consequences associated with inadequate fire design. Thus far, a significant research effort has been placed on the behaviour of steel structures in fire, resulting in a considerably improved understanding of the response. However, currently, the fire design of steel structures is typically performed using simple design equations that are mere adoptions of design formulae originally developed for room temperature structural steel design, which may not accurately capture the behaviour of steel structures in fire in some cases. Considering the complexity of the response of steel structures in fire and the current computational resources widely available to structural engineers in practice, it suffices to state that the adoption of more advanced analysis and design techniques can lead to significantly more accurate fire design of steel structures.

The current European structural steel fire design standard EN 1993-1-2 [1] and its upcoming version prEN 1993-1-2 [2] recommend simple and advanced calculation models for the fire design of steel structures. Simple calculation models, which are considerably more widely

adopted in practice, use simplified design methods that are built on conservative assumptions by extending room temperature structural steel design rules, while advanced calculation models are typically based on nonlinear finite element analysis [3], which can generally be performed with beam finite elements in practice. In both simple calculation models and advanced calculation models applied with beam finite elements, to account for local buckling effects in fire, the use of (i) the cross-section classification concept categorising cross-sections into discrete classes on the basis of the slenderness of their constituent elements and (ii) the effective width method [4,5] employed to assign effective widths to the elements of slender sections is necessary. However, this approach (i) does not capture the continuous relationship between capacity and cross-section slenderness which occurs in reality, (ii) disregards the interactions between cross-section elements in the consideration of local buckling, (iii) ignores partial plastification of cross-sections and (iv) has been found to result in rather inaccurate estimations of the resistances of steel members undergoing local buckling at elevated temperatures [6–12].

With the aim of establishing an advanced fire design method for steel structures which utilises the contemporary computational tools available to the structural engineering profession, a new structural

---

* Corresponding author.
*E-mail addresses:* hasan.murtaza@warwick.ac.uk (H. Murtaza), merih.kucukler@warwick.ac.uk (M. Kucukler).

steel fire design approach using second-order inelastic analysis with strain limits is put forward in this paper. The proposed design approach is applied to the fire design of steel columns as a first step in the establishment of a new design framework for structural steel fire design. The proposed method utilises computationally efficient beam finite elements to perform the second-order inelastic analysis of a steel structure or member in fire. Since conventional beam finite elements are not able to capture cross-section instability effects, strain limits derived from a modified continuous strength method (CSM) base curve [13,14] on the basis of the cross-section slenderness are used to represent the influence of local buckling on structural resistance. The design approach proposed in this paper extends the ambient temperature structural steel design approach using second-order inelastic analysis with strain limits developed in [15–19] to structural steel fire design.

In this paper, to enable the application of the proposed structural fire design approach using second-order inelastic analysis with strain limits, (i) the adoption of an appropriate elevated temperature material model is recommended and (ii) equivalent geometric imperfections suitable for the fire design of steel structures are put forward; (iii) thermal effects are considered during analysis and (iv) modifications are made to the CSM base curve to account for the nonlinear nature of the stress–strain response of steel in fire. Failure is defined within second-order inelastic analysis with strain limits as (i) the load or temperature at which the predefined strain limit is reached or (ii) the peak load or critical temperature achieved during analysis, whichever occurs first. The proposed design approach provides multiple benefits over the existing EN 1993-1-2 [1] fire design approaches. Member instabilities are captured explicitly during analysis, thereby precluding the requirement for member design checks. Since the structural analysis accounts for initial imperfections, geometric and material nonlinearities and thermal expansion directly, (i) changes in stiffness, (ii) failure modes and (iii) indirect fire actions resulting from the resistance to thermal expansion are very accurately modelled. Moreover, the adoption of the CSM strain limits in the analysis enables the consideration of the spread of plasticity in a manner which facilitates a continuous relationship between cross-section slenderness and deformation capacity. Nonlinear shell finite element models of steel columns capable of mimicking their response at elevated temperatures are developed and validated. The proposed approach is extensively verified against the benchmark results obtained from the validated shell finite element models, considering various cross-section and member slendernesses, cross-section shapes and elevated temperature levels. The accuracy of the existing fire design rules of EN 1993-1-2 [1] is also assessed. It is shown that the proposed design approach results in considerably improved accuracy in the fire design of steel columns relative to EN 1993-1-2 [1].

## 2. Traditional steel design at elevated temperatures

In traditional structural steel fire design, structural analysis is performed to determine the internal forces within the individual members of a steel structure, followed by design checks to assess the resistances of the individual members against these internal forces at elevated temperatures. The traditional simplified calculation models of EN 1993-1-2 [1] largely adopt the recalibrated design formulae of the European structural steel room temperature design standard EN 1993-1-1 [20] to determine the resistances of structural steel members in fire, taking into account the reduced strength and stiffness of steel at elevated temperatures. However, such an approach uses calculation models which make considerable simplifications such as largely excluding indirect fire actions (i.e. changes in internal forces due to restrained thermal expansion) and assuming uniform temperature distributions along the member lengths and through the cross-sections [3]. To avoid the shortcomings of the simplified calculation models, advanced calculation models may be used as indicated in EN 1993-1-2 [1]. In

this approach, advanced analysis (second-order inelastic analysis) using beam finite elements may be performed, accounting for initial member imperfections and residual stresses. However, the guidelines for the implementation of the advanced calculation models in structural steel fire design are rather limited in EN 1993-1-2 [1]; additionally, the design checks using the cross-section classification and effective width concepts may still be required to verify structural capacity.

In the fire design of steel columns, the simplified calculation model of EN 1993-1-2 [1] requires that the design axial compression force $N_{fi,Ed}$ should be less than or equal to the design buckling resistance $N_{b,fi,Rd}$ of the member at time $t$ with a uniform temperature $\theta_a$ (i.e. $N_{fi,Ed}/N_{b,fi,Rd} \leq 1.0$) to ensure that the steel column can withstand the applied axial compression $N_{fi,Ed}$ at the elevated temperature level $\theta_a$. Similar to EN 1993-1-1 [20], a buckling reduction factor $\chi_{fi}$ is used to account for column buckling, and cross-sections are classified depending on their susceptibility to local instability effects. The design buckling resistance of a steel column in fire $N_{b,fi,Rd}$ is determined as

$$N_{b,fi,Rd} = \frac{\chi_{fi} A k_{y,\theta} f_y}{\gamma_{M,fi}} \quad \text{for Class 1, 2 and 3 cross-sections}$$

$$N_{b,fi,Rd} = \frac{\chi_{fi} A_{eff} k_{p0.2,\theta} f_y}{\gamma_{M,fi}} \quad \text{for Class 4 cross-sections} \tag{1}$$

where $\gamma_{M,fi}$ is a partial factor for resistance in fire conditions, $f_y$ is the room temperature yield strength, $A$ is the gross cross-section area, $A_{eff}$ is the effective cross-section area calculated through the effective width concept provided in the room temperature steel plate design standard EN 1993-1-5 [21], $k_{y,\theta}$ is the elevated temperature yield strength reduction factor and $k_{p0.2,\theta}$ is the elevated temperature 0.2% proof strength reduction factor. As can be seen in Eq. (1), while the gross cross-section area $A$ and the elevated temperature material strength at 2% total strain $f_{2,\theta} = k_{y,\theta} f_y$ are used to determine the resistances of steel columns with Class 1, 2 and 3 cross-sections, the effective cross-section area $A_{eff}$ and the elevated temperature 0.2% proof strength $f_{p0.2,\theta} = k_{p0.2,\theta} f_y$ are employed in the calculation of the load carrying capacities of steel columns with Class 4 cross-sections. This highlights the assumption of a discrete relationship between column resistances and their susceptibility to local buckling effects in EN 1993-1-2 [1], which does not reflect the actual physical response. It should be noted that the described column design method in this section will henceforth be referred to as the EN 1993-1-2 [1] column design approach in this paper, considering that this is the most common EN 1993-1-2 [1] column design approach adopted in practice.

## 3. Structural steel fire design by second-order inelastic analysis with strain limits

In this section, the fundamental principles of the proposed fire design method by second-order inelastic analysis with strain limits are described. In the application of the proposed fire design method, the second-order inelastic analysis of a steel member or structure is performed through beam finite elements, taking into account the spread of plasticity through the volume of a steel member (i.e. plastic zone analysis).

### 3.1. Material model

To model the elevated temperature material response of steel in a second-order inelastic analysis whereby the proposed fire design method is applied, the four-stage EN 1993-1-2 [1] elevated temperature material model shown in Fig. 1(a) is adopted. The adopted four-stage EN 1993-1-2 [1] elevated temperature material model is given by Eq. (2):

$$\sigma = \begin{cases} \epsilon E_\theta & \text{for } \epsilon \leq \epsilon_{p,\theta} \\ f_{p,\theta} - c + (b/a)\sqrt{a^2 - (\epsilon_{2,\theta} - \epsilon)^2} & \text{for } \epsilon_{p,\theta} < \epsilon < \epsilon_{2,\theta} \\ f_{2,\theta} & \text{for } \epsilon_{2,\theta} < \epsilon < \epsilon_{t,\theta} \\ f_{2,\theta}[1 - (\epsilon - \epsilon_{t,\theta})/(\epsilon_{u,\theta} - \epsilon_{t,\theta})] & \text{for } \epsilon_{t,\theta} < \epsilon < \epsilon_{u,\theta} \\ 0 & \text{for } \epsilon = \epsilon_{u,\theta} \end{cases} \tag{2}$$

(a) Stress-strain response
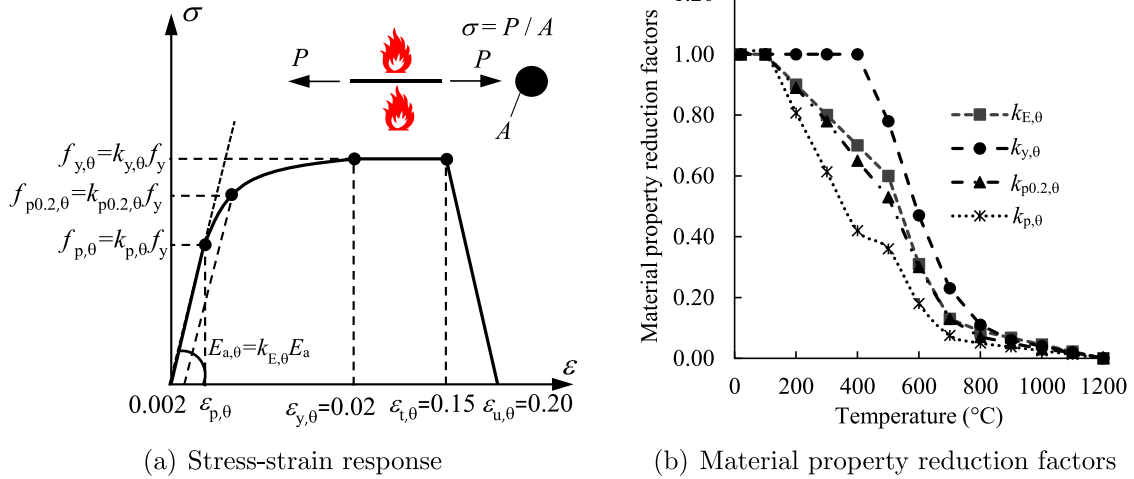


(b) Material property reduction factors

**Fig. 1.** Stress–strain relationship and material property reduction factors for carbon steel at elevated temperatures adopted in this study as given in [1].

where $\sigma$ and $\epsilon$ are the stress and strain, $E_\theta$ is the elevated temperature Young's modulus, $f_{p,\theta}$ is the elevated temperature proportional limit stress, $f_{2,\theta}$ is the elevated temperature material strength at 2% total strain, $\epsilon_{p,\theta}$ is the strain value at the proportional limit calculated as $\epsilon_{p,\theta} = f_{p,\theta}/E_\theta$, $\epsilon_{2,\theta}$ is the 2% total strain (i.e. $\epsilon_{2,\theta} = 0.02$), $\epsilon_{t,\theta}$ is the limit strain equal to 0.15 (i.e. $\epsilon_{t,\theta} = 0.15$) and $\epsilon_{u,\theta}$ is the ultimate strain taken as 0.20 (i.e. $\epsilon_{u,\theta} = 0.20$). Note that the elevated temperature Young's modulus $E_\theta$ is determined by multiplying the room temperature Young's modulus $E$ by the elevated temperature Young's modulus reduction factor $k_{E,\theta}$ (i.e. $E_\theta = k_{E,\theta}E$), while the elevated temperature proportional limit stress $f_{p,\theta}$ and material strength at 2% total strain $f_{2,\theta}$ are determined by multiplying the elevated temperature proportional limit stress reduction factor $k_{p,\theta}$ and yield strength reduction factor $k_{y,\theta}$ by the room temperature yield strength $f_y$ respectively (i.e. $f_{p,\theta} = k_{p,\theta}f_y$ and $f_{2,\theta} = k_{y,\theta}f_y$). In the proposed fire design approach, the material property reduction factors for stiffness and strength $k_{E,\theta}$, $k_{y,\theta}$, $k_{p0.2,\theta}$ and $k_{p,\theta}$ provided in EN 1993-1-2 [1] are adopted, whose variations with temperature are displayed in Fig. 1(b). Additionally, the coefficients $a$, $b$ and $c$ used in Eq. (2) are determined as given below in accordance with EN 1993-1-2 [1]:

$$
\begin{aligned}
a &= \sqrt{(\epsilon_{2,\theta} - \epsilon_{p,\theta})(\epsilon_{2,\theta} - \epsilon_{p,\theta} + c/E_\theta)}, \\
b &= \sqrt{c(\epsilon_{2,\theta} - \epsilon_{p,\theta})E_\theta + c^2}, \\
c &= \frac{(f_{2,\theta} - f_{p,\theta})^2}{(\epsilon_{2,\theta} - \epsilon_{p,\theta})E_\theta - 2(f_{2,\theta} - f_{p,\theta})}.
\end{aligned}
\tag{3}
$$

### 3.2. Cross-section slenderness

The proposed method requires the determination of the elevated temperature cross-section slenderness $\bar{\lambda}_{p,\theta}$ of a steel member, thereby enabling the consideration of the influence of the interactions between cross-section elements (e.g. flanges and webs) on its local buckling resistance. The elevated temperature cross-section slenderness $\bar{\lambda}_{p,\theta}$ of a steel member is determined through Eq. (4):

$$
\bar{\lambda}_{p,\theta} = \bar{\lambda}_p \sqrt{\frac{k_{p0.2,\theta}}{k_{E,\theta}}} = \sqrt{\frac{f_y}{\sigma_{cr,cs}}} \sqrt{\frac{k_{p0.2,\theta}}{k_{E,\theta}}},
\tag{4}
$$

in which $\sigma_{cr,cs}$ is the full cross-section elastic local buckling stress and $\bar{\lambda}_p$ is the room temperature cross-section slenderness. The full cross-section elastic local buckling stress $\sigma_{cr,cs}$ of a steel section can be determined using the formula proposed in Gardner et al. [22] as given by:

$$
\sigma_{cr,cs} = \sigma_{cr,p}^{SS} + \zeta \left( \sigma_{cr,p}^{F} - \sigma_{cr,p}^{SS} \right),
\tag{5}
$$

where $\sigma_{cr,p}^{SS}$ and $\sigma_{cr,p}^{F}$ are the minimum values of the elastic critical buckling stresses of the constituent plates of a steel section determined considering them in isolation with simply-supported and fixed boundary conditions, respectively. Moreover, $\zeta$ in Eq. (5) is the element interaction coefficient used to determine the interactions between cross-section elements during local buckling as described in [22]; $\zeta$ ranges between 0 and 1 (i.e. $0 \leq \zeta \leq 1$). Detailed information on the determination of the elastic local buckling stresses of full cross-sections $\sigma_{cr,cs}$ through Eq. (5) and element interaction coefficients $\zeta$ can be found in [22]. Note that the finite strip method software CUFSM [23] may also be employed to determine the full cross-section elastic local buckling stresses $\sigma_{cr,cs}$; in this paper, the practical formulae for the determination of the local buckling stresses of full cross-sections $\sigma_{cr,cs}$ proposed by Gardner at al. [22] is adopted in the implementation of the proposed fire design method.

### 3.3. Base curve

A fundamental aspect of the Continuous Strength Method (CSM) is a base curve which defines the peak compressive strain $\epsilon_{csm}$ a cross-section can withstand prior to its failure due to local buckling. The CSM base curve relates the cross-section slenderness $\bar{\lambda}_p$ to its deformation capacity $\epsilon_{csm}$, thereby accounting for the influence of the local geometric imperfections and local instabilities on the ultimate resistances of structural members. The CSM base curve was originally developed for stainless steel elements with non-slender cross-sections [14] and then extended to consider the response of slender cross-sections [24,25]; the base curve was also found to be applicable to the design of aluminium [25] and steel sections at room temperature [26] and elevated temperatures [27]. The CSM base curve is defined through Eq. (6) for non-slender cross-sections ($\bar{\lambda}_p \leq 0.68$) and Eq. (7) for slender cross-sections ($\bar{\lambda}_p > 0.68$) in terms of the local buckling strain $\epsilon_{csm}$ normalised by the yield strain $\epsilon_y$ (i.e. $\epsilon_{csm}/\epsilon_y$) as

$$
\frac{\epsilon_{csm}}{\epsilon_y} = \frac{0.25}{\bar{\lambda}_p^{3.6}} \leq \left( \Omega, \frac{C_1 \epsilon_u}{\epsilon_y} \right) \quad \text{for} \quad \bar{\lambda}_p \leq 0.68,
\tag{6}
$$

$$
\frac{\epsilon_{csm}}{\epsilon_y} = \left( 1 - \frac{0.222}{\bar{\lambda}_p^{1.05}} \right) \frac{1}{\bar{\lambda}_p^{1.05}} \quad \text{for} \quad 0.68 < \bar{\lambda}_p \leq 1.6.
\tag{7}
$$

The upper limits of $\Omega$ and $C_1 \epsilon_u/\epsilon_y$ are used for non-slender cross-sections. The upper limit $\Omega$ defines the maximum allowable level of plastic deformation, while the upper limit $C_1 \epsilon_u/\epsilon_y$ ensures that the overestimation of the material strength is avoided where $\epsilon_u$ is the ultimate strain and $C_1$ is a coefficient dependent on the adopted material model.
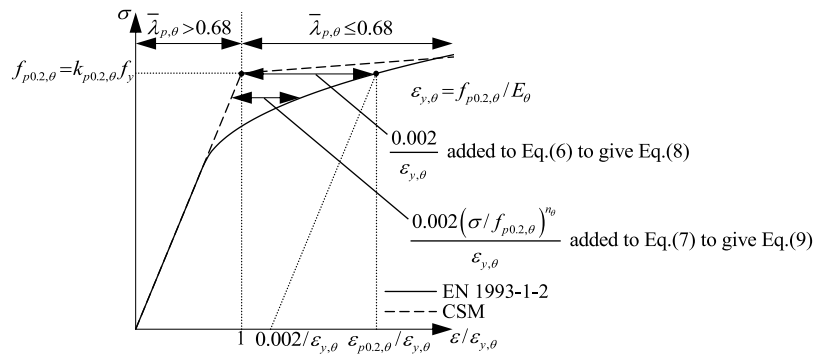
**Fig. 2.** Illustration of the required adjustments to the CSM base curve to reflect the change from the CSM elastic, linear hardening material model to the rounded EN 1993-1-2 [1] elevated temperature material model.

Considering isothermal experiments on stub columns with non-slender cross-sections, previous work [27] assessed the applicability of the room temperature CSM base curve for structural steel fire design through the reduction of the strength by the 0.2% proof strength reduction factor $k_{p0.2,\theta}$ (i.e. $f_{p0.2,\theta} = k_{p0.2,\theta} f_y$) and the stiffness by the Young's modulus reduction factor $k_{E,\theta}$ (i.e. $E_\theta = k_{E,\theta} E$). It was found that the ambient temperature CSM base curve provides a generally lower-bound fit to the test data. This is in agreement with the $k_{p0.2,\theta}$ and $k_{E,\theta}$ values provided in Fig. 1(b), illustrating that the 0.2% proof strength and Young's modulus of carbon steel generally reduce at a similar rate in fire. The ambient temperature CSM base curve was therefore adopted for design by second-order inelastic analysis with strain limits at elevated temperatures in this paper with a series of modifications. The CSM base curve given by Eqs. (6) and (7) was originally derived considering an elastic, linear hardening material model [14] to facilitate the implementation of the CSM through hand calculations. Since the fire design approach proposed in this paper uses a nonlinear elevated temperature stress–strain material model for steel as given by Eq. (2), the original CSM base curve has to be modified when it is used in the application of the proposed design method. To perform the adjustments in the CSM base curve in line with the procedure followed in Walport et al. [19], the two-stage Ramberg–Osgood [28,29] elevated temperature material model used in Kucukler et al. [30] for steel was calibrated to match the EN 1993-1-2 [1] elevated temperature material model up to the strain corresponding to the 0.2% proof strength $\epsilon_{p0.2,\theta}$ for different temperature levels; the calibration was carried out through calibrating the Ramberg–Osgood exponent $n_\theta$ as well as adopting the same elevated temperature material properties $E_\theta$, $f_{p0.2,\theta}$, and $\epsilon_{p0.2,\theta}$ provided in EN 1993-1-2 [1].

Fig. 2 illustrates the required changes in the original CSM base curve to reflect the move from the elastic, linear hardening CSM material model to the rounded EN 1993-1-2 [1] elevated temperature material model. In line with [19], (i) a constant strain equal to 0.2% is added to the base curve in the non-slender range (i.e. $\bar{\lambda}_{p,\theta} \leq 0.68$) considering that 0.2% strain was originally deducted from the actual local buckling strains obtained from experiments on steel sections with $\bar{\lambda}_{p,\theta} \leq 0.68$ during the development of the original CSM base curve [27] and (ii) a strain value varying with the stress level is added in the slender range (i.e. $\bar{\lambda}_{p,\theta} > 0.68$). The calibrated Ramberg–Osgood exponents $n_\theta$ relevant for the adjustment of the CSM base curve for temperatures between 200 °C and 1100 °C are shown in Table 1. Eqs. (8) and (9) provide the modified CSM base curve used in the application of the proposed second-order inelastic analysis with strain limits fire design approach:

$$\frac{\epsilon_{csm,\theta}}{\epsilon_{y,\theta}} = \frac{0.25}{\bar{\lambda}_{p,\theta}^{3.6}} + \frac{0.002}{\epsilon_{y,\theta}} \leq \left( \Omega, \frac{C_1}{\epsilon_{y,\theta}} \right) \quad \text{for} \quad \bar{\lambda}_{p,\theta} \leq 0.68, \tag{8}$$

$$\frac{\epsilon_{csm,\theta}}{\epsilon_{y,\theta}} = \left( 1 - \frac{0.222}{\bar{\lambda}_{p,\theta}^{1.05}} \right) \frac{1}{\bar{\lambda}_{p,\theta}^{1.05}} + \frac{0.002(\sigma/f_{p0.2,\theta})^{n_\theta}}{\epsilon_{y,\theta}}$$

$$\text{for} \quad 0.68 < \bar{\lambda}_{p,\theta} \leq 1.0, \tag{9}$$

**Table 1**
Strain hardening parameter $n_\theta$ values derived by fitting the Ramberg–Osgood material model [28] to the EN 1993-1-2 [1] material model for carbon steel.

| Temperature (°C) | $n_\theta$ |
|---|---|
| 200 | 38.40 |
| 300 | 14.82 |
| 400 | 7.38 |
| 500 | 8.52 |
| 600 | 6.59 |
| 700 | 5.42 |
| 800 | 8.44 |
| 900 | 16.10 |
| 1000 | 16.15 |
| 1100 | 15.82 |

where $\epsilon_{y,\theta}$ is the elevated temperature yield strain calculated as $\epsilon_{y,\theta} = f_{p0.2,\theta}/E_\theta$ and $\sigma$ is the maximum compressive stress. Note that $n_\theta$ in Eq. (9) can be determined from Table 1 for different elevated temperature levels. Similar to the other parameters of Eqs. (8) and (9), a linear interpolation can be adopted for temperature values not provided in Table 1. The upper limit $\Omega$ is set to 15 in accordance with the ductility requirements of EN 1993-1-1 [20] and $C_1$ is equal 0.02 which limits the maximum allowable strain to 2% in Eq. (8). The modified CSM curve used in the application of the proposed fire design approach is also graphically illustrated in Fig. 3. In line with [16], it is recommended to reduce the application range of Eq. (9) to $0.68 < \bar{\lambda}_{p,\theta} \leq 1.0$ in comparison to that of Eq. (7) which is equal to $0.68 < \bar{\lambda}_{p,\theta} \leq 1.6$ since Eq. (9) can be used in the fire design of structural systems while Eq. (7) is applied to individual steel members only. The reduction of the application range of Eq. (9) is recommended considering that significant local buckling effects may lead to pronounced stiffness reductions for structural systems with very slender sections (i.e. $\bar{\lambda}_{p,\theta} > 1.0$), which result in increased second-order effects. These increased second-order effects due to local buckling can only be captured through the modelling of structural systems by means of shell finite elements which is not computationally practical or adopting reduced stiffnesses for beam finite elements [31–33]. It should also be noted that as indicated, the proposed method uses a modified base curve which considers a continuous relationship between the elevated temperature cross-section deformation capacity $\epsilon_{csm,\theta}/\epsilon_{y,\theta}$, and the elevated temperature cross-section slenderness $\bar{\lambda}_{p,\theta} = \bar{\lambda}_p \sqrt{k_{p0.2,\theta}/k_{E,\theta}}$. Thus, the adopted base curve relies on the EN 1993-1-2 material property reduction factors including those specified for the elastic modulus $k_{E,\theta}$ and the 0.2% proof strength $k_{p0.2,\theta}$ in the determination of the elevated temperature cross-section deformation capacities $\epsilon_{csm,\theta}/\epsilon_{y,\theta}$ for structural steel elements in fire.

### 3.4. Equivalent geometric imperfections

To consider the influence of member imperfections (i.e. geometric member imperfections and residual stresses) on the behaviour of steel
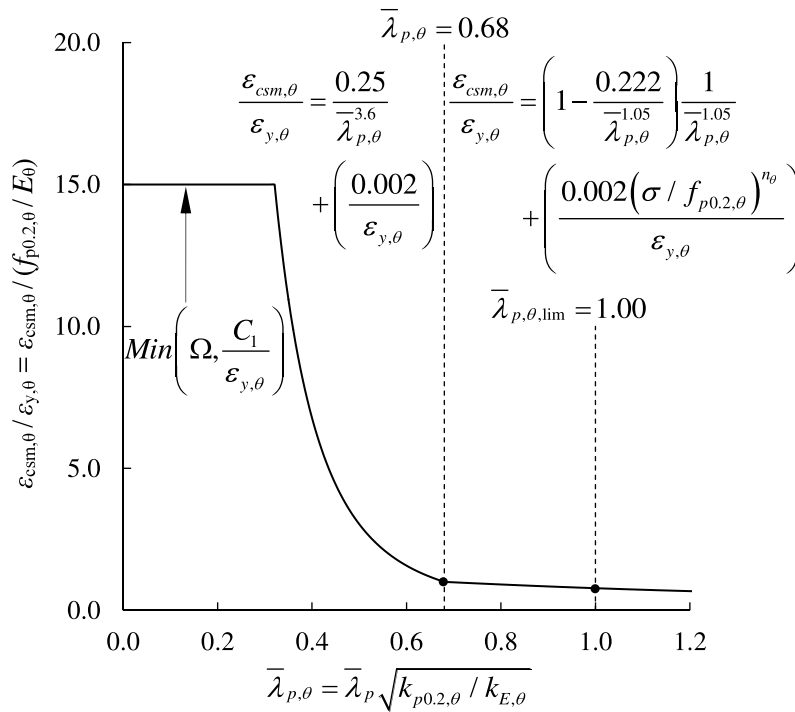
**Fig. 3.** Base curve modified for elevated temperature design relating the cross-section deformation capacity $\epsilon_{csm,\theta}/\epsilon_{y,\theta}$ to the elevated temperature cross-section slenderness $\overline{\lambda}_{p,\theta}$.

structures at elevated temperatures, the modelling of equivalent bow imperfections in steel members is recommended in the application of the proposed fire design approach. The equivalent geometric imperfections used in the proposed second-order inelastic analysis with strain limits fire design approach are determined as

$$e_0 = \alpha \beta L \geq L/1000 \quad \text{with} \quad \beta = \frac{1}{250}, \tag{10}$$

where $\alpha$ is the imperfection factor equal to $\alpha = 0.65\sqrt{235/f_y}$ from EN 1993-1-2 [1], $\beta = 1/250$ is the reference bow imperfection and $L$ is the member length; the lower bound to the equivalent imperfection $e_0$ is defined as $1/1000$ of the member length $L$ (i.e. $e_o = L/1000$) as this is the maximum permissible geometric member imperfection (i.e. member out-of-straightness) provided in the European standard for the execution of steel structures EN 1090-2 [34]. Note that the reference bow imperfection $\beta$ value of $1/250$ (i.e. $\beta = 1/250$) was determined through calibration in this study for the design of steel structures in fire, using the benchmark shell finite element models described in Section 4.1. This value is smaller than $\beta = 1/150$ recommended in [35] for the second-order inelastic analysis with strain limits room temperature structural steel design method since at elevated temperatures, the influence of residual stresses on the behaviour is less pronounced.

*3.5. Design procedure*

The procedure for fire design through second-order inelastic analysis with strain limits is shown in Fig. 4. A designer may opt for either the (i) isothermal analysis or (ii) anisothermal analysis approach. In the isothermal analysis approach, (i) initially, the temperature of the steel column is increased to a predefined value which is represented by the change of the stress–strain behaviour for the predefined elevated temperature level and (ii) then, the loading is applied up to failure. On the other hand, in the anisothermal analysis approach (also referred to as the transient-state analysis method), (i) initially, the loading is applied to the member at room temperature up to a fixed level and (ii) then, the temperature is increased, which leads to changes in the material behaviour as well as the development of thermal strains. Boundary conditions at the member ends may be (i) unrestrained where

the member is free to expand, (ii) axially restrained or (iii) axially and rotationally restrained. In both isothermal and anisothermal analysis techniques, the second-order inelastic analysis is performed using beam finite elements with the modelling of the equivalent bow imperfections calculated as described in Section 3.4. During the analysis, compressive mechanical strains are monitored within the member to define the load $F_{csm,\theta}$ or temperature $\theta_{csm}$ at the increment where the strain limit $\epsilon_{csm,\theta}$ is attained. When the isothermal analysis is used, the capacity of the column is defined as (i) the load at which the strain limit is reached $F_{csm,\theta}$ or (ii) the peak load $F_{peak,\theta}$ observed during the analysis, whichever comes first. On the other hand, in the anisothermal analysis method, the limit temperature of the column $\theta_{Rd}$ is defined as (i) the temperature at which the strain limit is reached $\theta_{csm}$ or (ii) the critical temperature $\theta_{cr}$ where a steel column cannot carry the applied loading as observed in the analysis, whichever occurs first. Although Fig. 4 shows the application of the proposed method to columns, a similar procedure is employed in the application of the proposed method to structural systems and frames where the second-order inelastic analysis of a structural system or frame in fire is conducted using beam finite elements. The strains in the structural system or frame are monitored to determine the failure temperature or load as (i) the temperature or load at which the strain limit is attained or (ii) the critical temperature or peak load observed during the advanced analysis, whichever occurs first. Research is currently underway to extend and illustrate the application of the proposed fire design method to structural systems and frames.

It is important to note that in the analyses of steel members and systems at elevated temperatures in the implementation of the proposed fire design approach, the total strains $\epsilon_t$ within steel sections can be expressed as

$$\epsilon_t = \epsilon_m + \epsilon_\theta, \tag{11}$$

in which $\epsilon_m$ are the mechanical strains and $\epsilon_\theta$ are the thermal strains; in the proposed method, initial strains do not exist within cross-sections due to the consideration of residual stresses through equivalent geometric imperfections and creep is implicitly incorporated into the EN 1993-1-2 [1] elevated temperature material model given by Eq. (2)
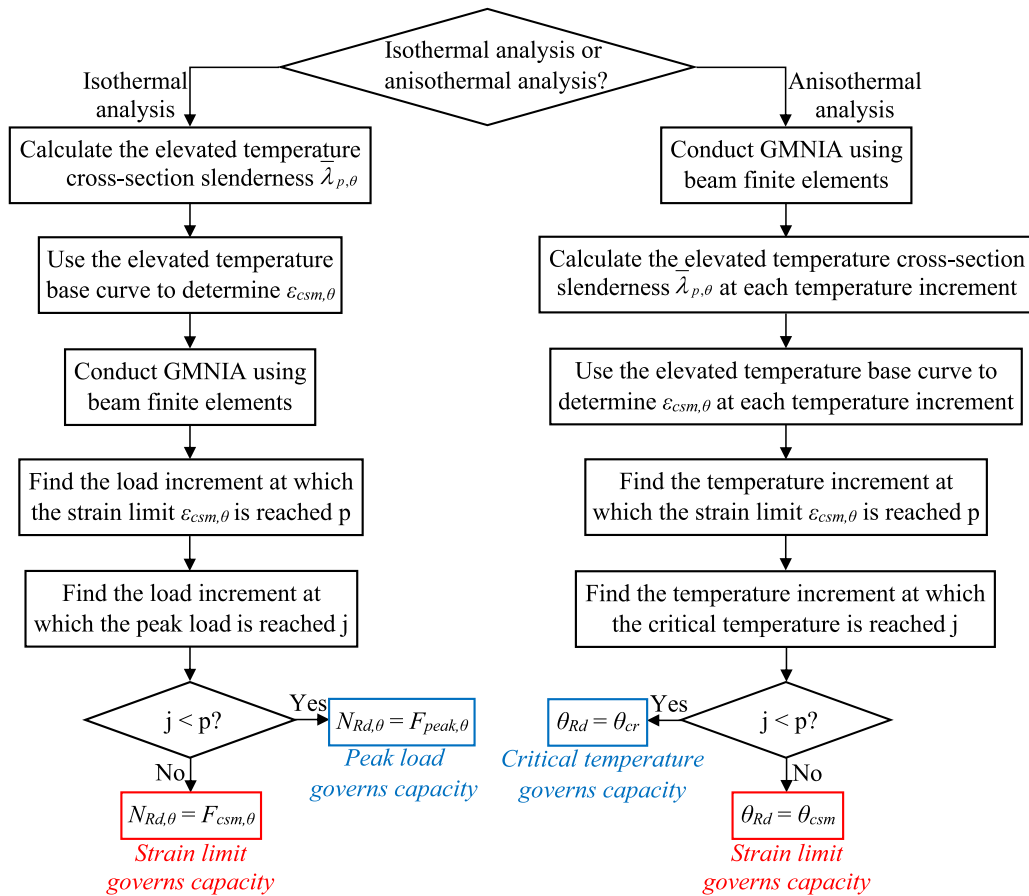
**Fig. 4.** Procedure for the design of steel columns through second-order inelastic analysis with strain limits at elevated temperatures.
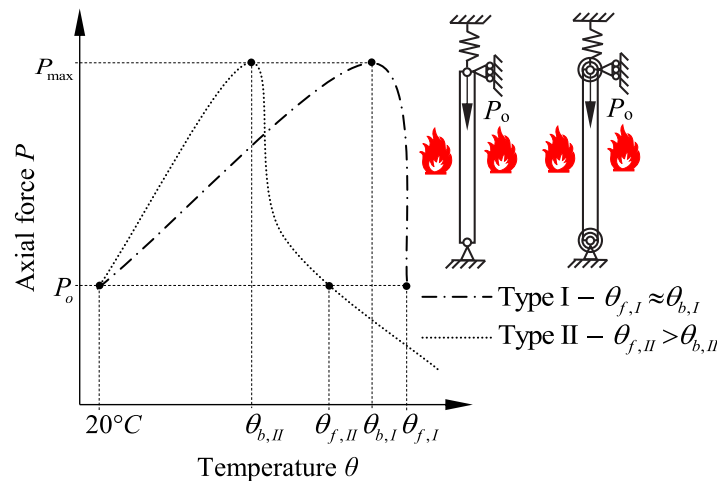


**Fig. 5.** Response of axially restrained columns subject to anisothermal analysis conditions.

in line with the recommendations of [36]. In the application of the proposed method, only the mechanical strains $\epsilon_m$ within structural steel sections have to be monitored and checked against the CSM strain limits $\epsilon_{csm,\theta}$ (i.e. $\epsilon_m \leq \epsilon_{csm,\theta}$) determined by Eqs. (8) and (9). The rationale behind this is that (i) the modified CSM base curve given by Eqs. (8) and (9) has been derived considering the mechanical strains in steel sections from isothermal fire experiments and (ii) the stresses within steel sections are directly dependent upon the mechanical strains $\epsilon_m$ in the finite element analyses of steel members and systems. The thermal strains $\epsilon_\theta$ developing within steel members with increasing temperatures are typically tensile strains and can be readily determined

taking into consideration material thermal expansion coefficients and elevated temperature levels. Finite element analysis software such as Abaqus [37] readily provides mechanical strains $\epsilon_m$ and thermal strains $\epsilon_\theta$ within steel sections individually, thereby enabling the application of the proposed method in a straightforward way.

Owing to their particular structural response, it is worthwhile discussing the behaviour of axially restrained steel columns analysed through the anisothermal analysis technique in the application of the proposed fire design method. The change in the internal force $P$ of an axially restrained steel column analysed through the anisothermal analysis technique is shown in Fig. 5, where (i) the buckling temperature

$\theta_b$ is defined as the temperature when the axial load in the column reaches a maximum value $P_{max}$ (i.e. $P = P_{max}$) and (ii) the failure temperature $\theta_f$ is defined as the temperature at which the axial load in the column returns to its original value prior to heating $P_o$ (i.e. $P = P_o$) after which the column cannot withstand the applied axial load $P_o$. As can be seen in Fig. 5, two types of failure may occur during an anisothermal analysis [38]: (i) Type I failure where the post-bucking behaviour is minimal or non-existent ($\theta_f \approx \theta_b$) or (ii) Type II failure typically involving higher degrees of restraint causing the column to exhibit a post-buckling response ($\theta_f > \theta_b$). In the application of the proposed fire design method to axially restrained columns with the anisothermal analysis technique, it is recommended to take the failure temperature $\theta_f$ as the critical temperature $\theta_{cr}$ in all cases and failure modes (i.e. $\theta_{cr} = \theta_f$).

Finally, in the implementation of the proposed fire design method in this study, the finite element analysis software Abaqus [37] was employed to perform the second-order inelastic analyses of steel columns, using the two-noded shear deformable prismatic Timoshenko beam elements B31OS and B31 for columns with I-sections and those with square and rectangular hollow sections (SHS & RHS), respectively. It should be emphasised that any other software package able to perform second-order inelastic analysis with beam finite elements can also be utilised in the application of the proposed fire design approach, provided that (i) the spread of plasticity through the cross-section depths and along the member lengths is taken into account, (ii) the second-order $P-\Delta$ and $P-\delta$ effects are considered and (iii) the temperature development can be modelled through the modification of the material behaviour and the development of thermal strains. Structural analysis software packages with these capabilities such as [39–41] are currently available to the structural engineering profession in practice, thus enabling the application of the proposed fire design approach.

## 4. Finite element modelling

This section describes the development and validation of the shell finite element modelling approach adopted to simulate the behaviour of steel columns at elevated temperatures in this paper. The validated shell finite element models are used in the subsequent sections to verify the proposed second-order inelastic analysis with strain limits fire design approach and assess its accuracy against the design provisions of EN 1993-1-2 [1].
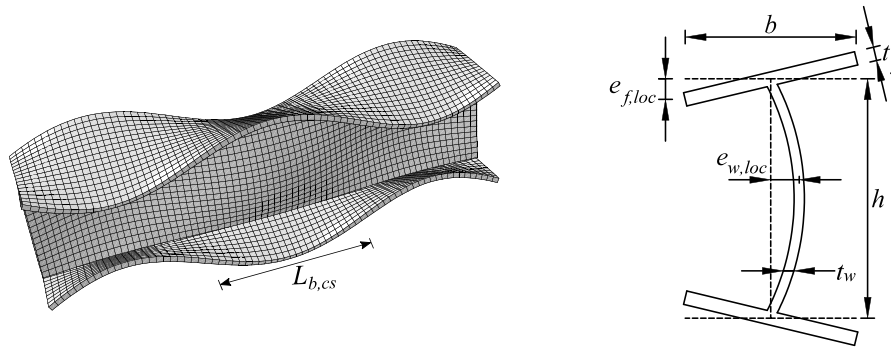
### 4.1. Development of shell finite element models

The finite element analysis software Abaqus [37] was used to create shell finite element models capable of replicating the structural response of steel columns in fire. The four-noded general purpose reduced integration shell element designated as S4R in the Abaqus element library was utilised to create all the shell finite element models. The Simpson integration method was employed with five integration points through the thickness of an element. To accurately capture the behaviour of columns, twelve S4R elements were used to model each constituent plate of the cross-section, while the number of elements in the longitudinal direction were defined such that an aspect ratio of approximately unity was achieved. The Poisson's ratio $v$ was taken as 0.3 (i.e. $v = 0.3$) in the elastic stress range, while it was defined as 0.5 (i.e. $v = 0.5$) in the plastic stress range [15,16]. To avoid the overlapping of the flange and web plates in the finite element models of steel columns with I-sections, the web nodes were offset by half the flange thicknesses in accordance with [42]. The EN 1993-1-2 [1] elevated temperature material model for carbon steel was used in the finite element models in conjunction with the corresponding material reduction factors as described in Section 3.1. The engineering stress–strain curves were converted into true stress–strain curves and then used in the finite element models. Member and local geometric imperfections were directly modelled in the shell finite element models

by manually defining the shapes and incorporating specified imperfection magnitudes into the models. The member out-of-straightness was modelled as a half-sine wave with a magnitude of $1/1000$ of the member length $L$ at mid-height. A series of sinusoidal curves were used to define local cross-section imperfections as shown in Fig. 6 (a) and (b), adopting local buckling half-wavelengths $L_{b,cs}$ determined in accordance with the method proposed in [43]. The local geometric imperfection magnitudes $e_0$ were taken as $1/200$ of the plate widths (i.e. $e_0 = b/200$) in accordance with [15,19] and then applied to the cross-section element with the lowest elastic critical buckling stress $\sigma_{cr}$; the local imperfection magnitude of the cross-section element with the higher elastic buckling stress was defined such that the 90° angle at the plate junctions was retained. In this study, the residual stresses were defined in the finite element models of steel columns with hot-rolled and welded I-sections as shown in Fig. 7, adopting the European Convention for Constructional Steelwork (ECCS) residual stress patterns [44]. Note that $f_{y,235}$ is a fixed residual stress magnitude for hot-rolled sections equal to 235 MPa regardless of the steel grade in accordance with [44]. In the case of hot-rolled square hollow sections (SHS) and rectangular hollow sections (RHS), residual stresses were not explicitly modelled because of their negligible influence on ultimate resistance [45].

Shell finite element models were analysed adopting both isothermal and anisothermal analysis techniques, thereby verifying the proposed fire design approach for both analysis methods. An isothermal analysis was conducted using the following steps: (i) the application of the residual stresses at room temperature for the I-section models (for the SHS & RHS models, this step is skipped), (ii) the incremental increase of the temperature up to a predefined elevated temperature level resulting in the development of thermal strains and the modification of the stress–strain response and finally, (iii) the application of the axial compression to the column up to failure; in the last step, the second-order inelastic analysis was performed adopting the modified Riks method [47,48] which allow the full load–displacement response to be traced including the post-ultimate response. In the case of an anisothermal analysis, a different technique was adopted. Prior to conducting an anisothermal analysis, a heat transfer analysis was performed to determine the temperature development within a steel column with respect to time due to fire exposure. An ambient temperature increase was performed using the standard ISO 834 temperature–time curve [1], resulting in a uniform temperature development in the steel column. Properties such as the specific heat, thermal conductivity and thermal expansion were specified in accordance with EN 1993-1-2 [1]; the convective heat transfer coefficient $\alpha_c$ and emissivity factor $\epsilon_m$ were taken as 25 W/m² K and 0.7 as recommended in [1]. An anisothermal analysis was then performed through the following steps: (i) the application of the residual stresses at room temperature for the I-section models (for the SHS & RHS models this step is skipped), (ii) the application of a predefined axial load $N_{Ed}$ to the column at room temperature and finally, (iii) the incremental application of a uniform temperature increase to the column up to failure on the basis of the temperature–time relationship obtained from a prior heat transfer analysis. The predefined axial load $N_{Ed}$ applied to a steel column in an anisothermal analysis is defined taking into account a parameter referred to as the axial load intensity $\alpha_N$ which is equal to the ratio of the applied axial load $N_{Ed}$ to the room temperature design buckling resistance $N_{b,Rd}$ determined in accordance with the European room temperature structural steel design standard EN 1993-1-1 [20] (i.e. $\alpha_N = N_{Ed}/N_{b,Rd}$).

To prevent localised yielding and buckling at the end supports and load application points, all the nodes at the end sections were constrained to the reference nodes located at the centroids of the end sections through kinematic coupling constraints, where the boundary conditions were defined and the loading was applied. In Fig. 8, the boundary conditions for the axially and rotationally unrestrained, axially restrained and axially and rotationally restrained I-section columns undergoing minor axis flexural buckling in fire are displayed, where $\Delta$
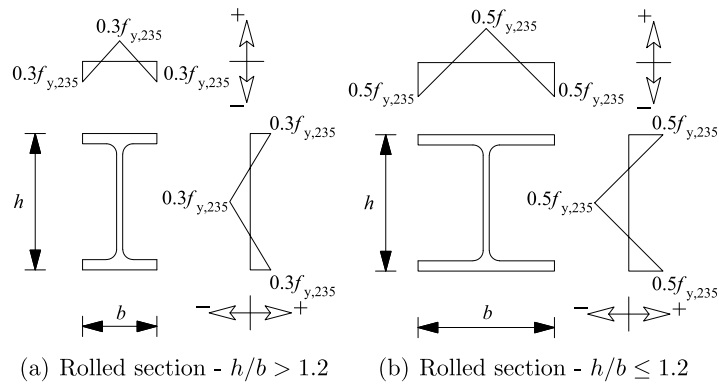
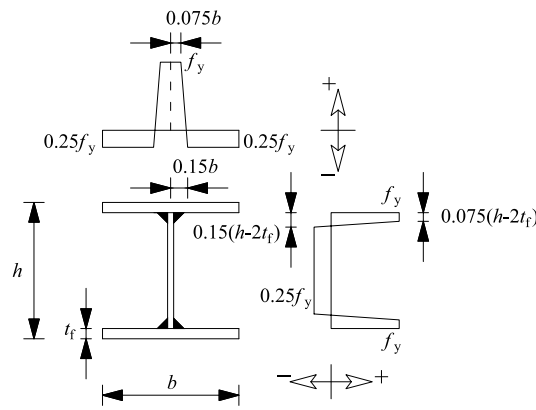(a) Local imperfections for I-sections
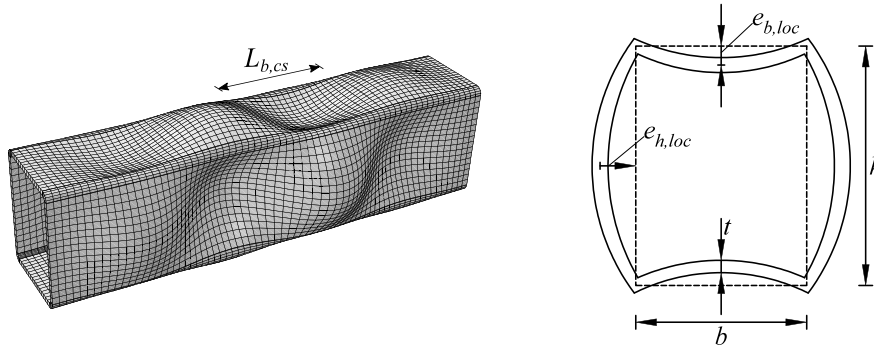


(b) Local imperfections for SHS/RHS

**Fig. 6.** Local geometric imperfections used within shell finite element models.



(a) Rolled section - $h/b > 1.2$

(b) Rolled section - $h/b \leq 1.2$



(c) Welded section

**Fig. 7.** ECCS residual stress patterns [44] used in the shell finite element models.
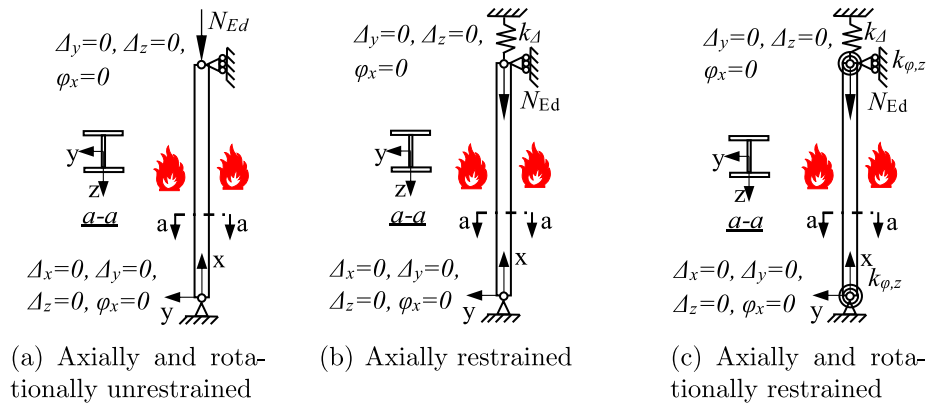
**Fig. 8.** Support conditions adopted for unrestrained and restrained I-section columns undergoing minor axis flexural buckling in fire.
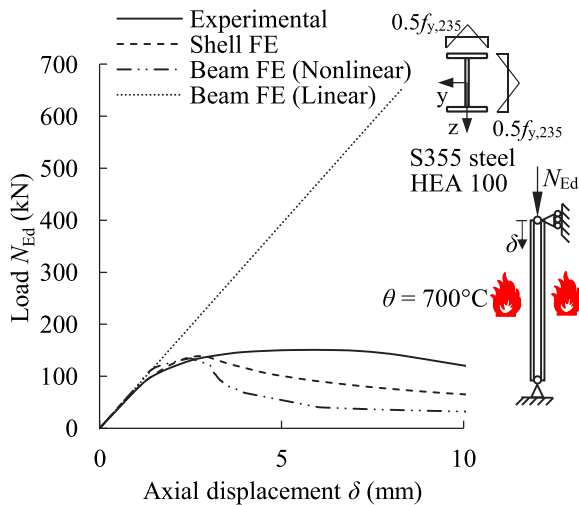


**Fig. 9.** Comparison between axial load versus end-shortening paths from the Pauli et al. [46] isothermal fire test and shell and beam finite element models for a hot-rolled HEA 100 column.

and $\varphi$ are the translation and rotation with respect to the corresponding axis respectively, $k_\Delta$ is the axial spring stiffness of the translational spring used to define the level of axial restraint and $k_\varphi$ is the rotational spring stiffness of the rotational springs employed to define the level of rotational restraints at the supports about the buckling axis. The same boundary conditions were also adopted for the SHS & RHS columns and I-section columns undergoing major axis buckling, defining the rotational stiffnesses with respect to the corresponding buckling axis. In addition to the boundary conditions shown in Fig. 8, the lateral translations in the out-of-plane direction were also suppressed at the web-to-flange junctions along the lengths of members for the RHS and I-section columns undergoing major axis flexural buckling so that the major axis flexural buckling mode is induced. Spring stiffnesses were specified using an axial restraint stiffness ratio $\alpha_\Delta$ and rotational restraint stiffness ratio $\alpha_\varphi$ defined in Eqs. (12) and (13) as

$$\alpha_\Delta = \frac{k_\Delta}{EA_c/L}, \tag{12}$$

$$\alpha_\varphi = \frac{k_\varphi}{4EI_c/L}, \tag{13}$$

where $k_\Delta$ is the axial spring stiffness, $k_\varphi$ is the rotational spring stiffness, $L$ is the column length, $A_c$ is the cross-section area of the column and $I_c$ is the second-moment of area of the column cross-section about the buckling axis.

## 4.2. Validation of shell finite element models

Results from fire tests on steel columns from the literature were used to validate the shell finite element models used in this paper. The geometric and material properties, support conditions and the imperfection magnitudes of the specimens reported in the considered experimental studies were used within the models. Where the complete stress–strain material response of a specimen was not provided, the EN 1993-1-2 [1] material model was adopted. Similarly, where the geometric imperfections were not directly measured, the imperfection magnitudes described in Section 4.1 were used. It should be noted that the finite element modelling approach adopted in this paper has also been extensively validated previously in [30,42,49–52].

### 4.2.1. Validation against isothermal experiments carried out on I-section and SHS and RHS columns and stub columns

Pauli et al. [46] and Wang et al. [53] performed fire experiments on I-section steel columns and stub columns adopting the isothermal testing method where the specimens were first heated up to predefined temperature levels and then loaded up to failure. In [46], the tests were carried out on hot-rolled HEA 100 columns and stub columns at 400 °C, 550 °C and 700 °C, while the fire experiments were conducted on welded I-section columns at 450 °C and 650 °C in [53]. The ECCS [44] residual stress pattern for welded I-sections was used in the finite element models of the welded columns tested in [53]. The ultimate axial load carrying capacities of the columns observed in the experiments $N_{u,test}$ and those determined through the shell finite element models $N_{u,FE}$ are compared in Tables 2 and 3, where $L$ is the specimen length and $\theta$ is the temperature level. As can be seen in Tables 2 and 3, there is a good agreement between the ultimate capacity predictions observed in the experiments and those obtained from the numerical models, indicating the capability of the adopted shell finite element approach in replicating the structural response of I-section columns and stub columns in fire.

The experimental programme of Pauli et al. [46] included the isothermal fire testing of grade S355 hot-rolled SHS and RHS columns and stub columns which were also used for the validation of the finite element modelling approach adopted for hollow section columns. Table 4 shows the ultimate axial load carrying capacities observed during the experiments $N_{u,test}$ and those obtained from the finite element models $N_{u,FE}$. As can be seen from the table, the shell finite element models provide ultimate load capacities close to those observed in the experiments of [46] on hollow section columns and stub columns in fire, which highlights the shell finite element models are able to mimic the structural response of hollow section steel columns in fire.

Additionally, Fig. 9 shows the load–displacement path of an HEA 100 column from the Pauli et al. [46] experiments as well as the load–displacement paths obtained using the benchmark shell finite element model and beam finite element model of the steel column created

**Table 2**

Comparison of the ultimate resistances of I-section steel columns obtained from the shell finite element models against those observed in the fire experiments of Pauli et al. [46].

| Test | Specimen | Buckling axis | $L$ (m) | $\theta$ (°C) | $N_{u,test}$ (kN) | $N_{u,FE}$ (kN) | $N_{u,FE}/N_{u,test}$ |
|------|----------|---------------|---------|---------------|-------------------|-----------------|------------------------|
| HEA100_Stub_400C | S19 | – | 0.34 | 400 | 996 | 894 | 0.90 |
| HEA100_Stub_550C | S13 | – | 0.34 | 550 | 511 | 431 | 0.84 |
| HEA100_Stub_700C | S22 | – | 0.34 | 700 | 162 | 154 | 0.95 |
| HEA100_M_400C_z0 | M02 | z | 0.85 | 400 | 646 | 610 | 0.94 |
| HEA100_M_550C_z0 | M03 | z | 0.85 | 550 | 405 | 365 | 0.90 |
| HEA100_SL_400C_y0 | L08 | y | 1.88 | 400 | 608 | 555 | 0.91 |
| HEA100_SL_400C_z0 | L016 | z | 1.88 | 400 | 466 | 415 | 0.89 |
| HEA100_SL_550C_y0 | L07 | y | 1.88 | 550 | 395 | 346 | 0.87 |
| HEA100_SL_550C_z0 | L011 | z | 1.88 | 550 | 297 | 262 | 0.88 |
| HEA100_SL_700C_y0 | L01 | y | 1.88 | 700 | 152 | 139 | 0.91 |
| HEA100_SL_700C_z0 | L012 | z | 1.88 | 700 | 128 | 111 | 0.86 |
| **Average** | | | | | | | **0.90** |
| **COV** | | | | | | | **0.034** |

**Table 3**

Comparison of the ultimate resistances of I-section steel columns obtained from the shell finite element models against those observed in the fire experiments of Wang et al. [53].

| Section | Grade | $L$ (m) | $\theta$ (°C) | $N_{u,test}$ (kN) | $N_{u,FE}$ (kN) | $N_{u,FE}/N_{u,test}$ |
|---------|-------|---------|---------------|-------------------|-----------------|------------------------|
| I-250 × 250 × 6 × 8 | Q235 | 1.70 | 450 | 930 | 886 | 0.95 |
| I-250 × 250 × 6 × 8 | Q235 | 1.70 | 650 | 295 | 298 | 1.01 |
| I-316 × 200 × 6 × 8 | Q235 | 1.70 | 450 | 830 | 817 | 0.98 |
| I-316 × 200 × 6 × 8 | Q235 | 1.70 | 650 | 280 | 279 | 0.99 |
| I-250 × 220 × 8 × 8 | Q460 | 1.70 | 450 | 1640 | 1665 | 1.02 |
| I-250 × 220 × 8 × 8 | Q460 | 1.70 | 650 | 430 | 454 | 1.06 |
| I-336 × 160 × 8 × 8 | Q460 | 1.70 | 450 | 1450 | 1185 | 0.82 |
| I-336 × 160 × 8 × 8 | Q460 | 1.70 | 650 | 430 | 415 | 0.96 |
| **Average** | | | | | | **0.97** |
| **COV** | | | | | | **0.068** |

**Table 4**

Comparison of the ultimate resistances of hollow section steel columns obtained from the shell finite element models against those observed in the fire experiments of Pauli et al. [46].

| Test | Specimen | Buckling axis | $L$ (m) | $\theta$ (°C) | $N_{u,test}$ (kN) | $N_{u,FE}$ (kN) | $N_{u,FE}/N_{u,test}$ |
|------|----------|---------------|---------|---------------|-------------------|-----------------|------------------------|
| SHS160_Stub_400C | S3 | – | 0.52 | 400 | 795 | 740 | 0.93 |
| SHS160_Stub_550C | S6 | – | 0.52 | 550 | 468 | 435 | 0.93 |
| SHS160_Stub_700C | S5 | – | 0.52 | 700 | 138 | 119 | 0.86 |
| SHS160_SL_400C | L2 | – | 1.88 | 400 | 760 | 665 | 0.88 |
| SHS160_SL_550C | L5 | – | 1.88 | 550 | 467 | 406 | 0.87 |
| SHS160_SL_700C | L6 | – | 1.88 | 700 | 130 | 109 | 0.84 |
| RHS120_Stub_400C | S02 | – | 0.34 | 400 | 408 | 363 | 0.89 |
| RHS120_Stub_550C | S03 | – | 0.34 | 550 | 257 | 221 | 0.86 |
| RHS120_Stub_700C | S06 | – | 0.34 | 700 | 74 | 70 | 0.94 |
| RHS120_SL_400C_z0 | L08 | z | 1.88 | 400 | 242 | 193 | 0.80 |
| RHS120_SL_550C_z0 | L10 | z | 1.88 | 550 | 186 | 159 | 0.85 |
| RHS120_SL_700C_z0 | L05 | z | 1.88 | 700 | 71 | 69 | 0.97 |
| **Average** | | | | | | | **0.88** |
| **COV** | | | | | | | **0.054** |

in this study. The load–displacement path from beam finite element analysis using a linear elastic material response is also included in the figure. As can be seen from Fig. 9, the significant difference between the load–displacement paths obtained through the materially nonlinear and linear beam finite element analyses clearly demonstrates the importance of the consideration of the material nonlinearity. Fig. 9 also shows that the experimental and numerical load–displacement paths obtained through the shell and beam finite element models match well, thereby verifying the accuracy of the finite element models in capturing the structural response of steel columns at elevated temperatures.

### 4.2.2. Validation against anisothermal experiments carried out on unrestrained and restrained I-section columns

The anisothermal fire tests conducted by Dumont et al. [54] on hot-rolled and welded I-section steel columns are used to validate the shell finite element modelling approach adopted in this study with the aim of ensuring its accuracy when the anisothermal analysis approach is adopted. In the anisothermal fire tests of Dumont et al. [54], the specimens were first subjected to axial loading and then heated up to failure;

the experimental programme involved the eccentric axial loading of the columns with simply-supported end conditions, which facilitated either major or minor axis flexural buckling. Table 5 shows the comparisons of the critical temperatures observed in the experiments $\theta_{cr,test}$ and those determined by the shell finite element models $\theta_{cr,FE}$. As can be seen from Table 5, there is a good correlation between the critical temperatures observed in the experiments and those obtained from the shell finite element models, verifying the accuracy of the shell finite element models in replicating the behaviour of I-section steel columns in fire under the anisothermal testing conditions.

Finally, to validate the adopted shell finite element modelling approach for the case of the anisothermal analysis of restrained members, the Correia and Rodrigues [55] anisothermal tests on axially and rotationally restrained I-section steel columns were used. Heat transfer analyses using the standard ISO 834 temperature–time curve [1] were performed for the Correia and Rodrigues [55] tests as the temperature development within all the columns was not reported in [55]. The axial load intensities of the specimens $\alpha_N$ calculated as the ratio of the applied load $N_{Ed}$ to the room temperature design buckling resistance

**Table 5**

Comparison of the critical temperatures of I-section steel columns obtained from the shell finite element models against those observed in the fire experiments of Dumont et al. [54].

| Section | Type | $L$ (m) | Buckling axis | $\theta_{cr,test}$ (°C) | $\theta_{cr,FE}$ (°C) | $\theta_{cr,FE}/\theta_{cr,test}$ |
|---|---|---|---|---|---|---|
| IPE240A | Hot-rolled | 2.70 | z | 610 | 597 | 0.98 |
| 450 × 150 × 5 × 4 | Welded | 2.70 | z | 608 | 580 | 0.95 |
| 450 × 150 × 5 × 4 | Welded | 2.70 | z | 452 | 408 | 0.90 |
| 360 × 150 × 5 × 4 | Welded | 2.70 | y | 509 | 523 | 1.03 |
| 360 × 150 × 5 × 4 | Welded | 2.70 | y | 530 | 532 | 1.00 |
| HE340AA | Hot-rolled | 2.70 | y | 623 | 613 | 0.98 |
| **Average** | | | | | | **0.98** |
| **COV** | | | | | | **0.040** |

**Table 6**

Parameters used in the investigation of the accuracy of the proposed design approach for steel columns analysed adopting the isothermal analysis method.

| Cross-sections and loading conditions | | | Cross-section slenderness $\overline{\lambda}_{p,\theta}$ | Member slenderness $\overline{\lambda}_{\theta}$ | Temperature $\theta$ (°C) |
|---|---|---|---|---|---|
| | | | 0.2–1.1 | 0.5, 1.0, 1.5 | 300, 500, 700 |



$N_{b,Rd}$ according to EN 1993-1-1 [20] (i.e. $\alpha_N = N_{Ed}/N_{b,Rd}$) were equal to 30% and 70% (i.e. $\alpha_N = 0.30$ and 0.70). Different axial restraint ratios $\alpha_\Delta$ equal to the ratio of the axial restraint stiffness $k_\Delta$ to the axial stiffness of the column $EA_c/L$ (i.e. $\alpha_\Delta = k_\Delta/(EA_c/L)$) were adopted in the experiments, ranging from 0.035 to 0.473 (i.e. $\alpha_\Delta = 0.035 - 0.473$). In addition to the axial restraints, the Correia and Rodrigues [55] experiments included rotational restraints at the column ends based on the rotational stiffness of the structure surrounding the column. Fig. 10 shows the comparison of the axial displacement–temperature paths of the columns with HEA 200 and HEA 160 sections from the Correia and Rodrigues [55] experiments and those obtained from the finite element models. As can be seen from the figure, the experimental and numerical displacement versus temperature paths are very close, verifying the accuracy of the shell finite element models in mimicking the structural response of axially and rotationally restrained steel columns in fire in anisothermal testing conditions.

## 5. Assessment of the accuracy of the proposed design method

In this section, the accuracy of the proposed second-order inelastic analysis with strain limits fire design approach is assessed using the benchmark structural performance data generated through the validated shell finite element models. Design predictions from the simplified calculation models of EN 1993-1-2 [1] are also presented to demonstrate the significant advantages of the proposed method relative to traditional fire design.

### 5.1. Members subjected to compression analysed using the isothermal analysis method

The accuracy of the proposed method is assessed in this subsection for the fire design of steel columns analysed adopting the isothermal analysis method. The considered parameters in the verification of the proposed design approach when applied through the isothermal analysis technique are summarised in Table 6. An extensive parametric study is carried out considering (i) three cross-section types: I-sections, square and rectangular hollow sections (SHS & RHS); (ii) major and minor axis flexural buckling; (iii) hot-rolled and welded sections; (iv) elevated

temperature cross-section slenderness $\overline{\lambda}_{p,\theta}$ values ranging between 0.2 and 1.1 which comprises Class 1 to Class 4 cross-sections; (v) three elevated temperature levels of 300 °C, 500 °C and 700 °C and (vi) three elevated temperature column slenderness $\overline{\lambda}_{\theta}$ values equal to 0.5, 1.0 and 1.5 (i.e. $\overline{\lambda}_{\theta} = 0.5, 1.0, 1.5$) where $\overline{\lambda}_{\theta}$ is calculated as

$$\overline{\lambda}_{\theta} = \overline{\lambda}\sqrt{\frac{k_{y,\theta}}{k_{E,\theta}}} = \sqrt{\frac{Af_y}{N_{cr}}}\sqrt{\frac{k_{y,\theta}}{k_{E,\theta}}}, \tag{14}$$

in which $N_{cr}$ is the room temperature elastic critical flexural buckling load determined considering the corresponding buckling axis. Keeping the cross-section depths $h$ and widths $b$ constant for all the considered I-sections, SHS and RHS, the plate thicknesses of the cross-section elements were changed to obtain different cross-section slendernesses $\overline{\lambda}_{p,\theta}$ ranging between 0.2 and 1.1 (i.e. $0.2 < \overline{\lambda}_{p,\theta} < 1.1$). The flange and web thicknesses of the I-sections were selected such that the plate slendernesses of the web plates $\overline{\lambda}_{p,w}$ and flange plates $\overline{\lambda}_{p,f}$ determined considering them individually with simply-supported boundary conditions were essentially identical (i.e. $\overline{\lambda}_{p,w} = \overline{\lambda}_{p,f}$), thereby considering the most critical local buckling scenario for the I-sections with the most limited interactions between the cross-section elements. This was, of course, also the case for the columns with SHS which represented the most critical local buckling scenario for hollow sections. The steel grade was taken as grade S355 in the numerical simulations. Note that the proposed method will be further extended in the future to cover the fire design of high strength steel columns and steel columns with monosymmetric and unsymmetric sections.

Figs. 11–14 show the accuracy of the proposed fire design method against the benchmark capacity predictions determined through the shell finite element models for hot-rolled and welded I-section columns, RHS columns and SHS columns where $\overline{\lambda}_{y,\theta}$ and $\overline{\lambda}_{z,\theta}$ are the elevated temperature column slendernesses for major and minor axis flexural buckling respectively. In the figures, the design resistance predictions obtained from the shell finite element models and the proposed method $N_{Rd,\theta}$ are normalised by the elevated temperature 0.2% proof strength $f_{p0.2,\theta}$ multiplied by the cross-sectional area of the column $A$ (i.e. $N_{Rd,\theta}/(Af_{p0.2,\theta})$) and shown for different elevated temperature cross-section slendernesses $\overline{\lambda}_{p,\theta}$. In the ultimate strength predictions determined through the proposed second-order inelastic analysis with strain

(a) HEA 200 - Minor axis buckling
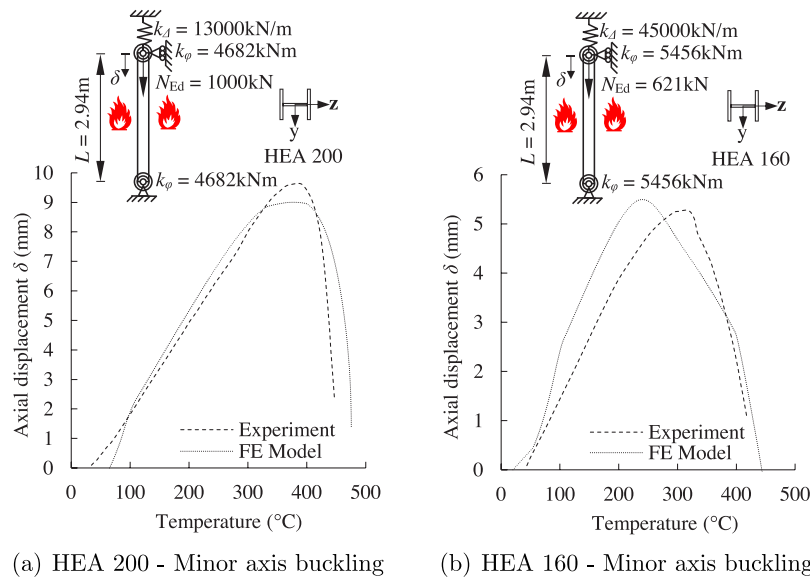


(b) HEA 160 - Minor axis buckling

**Fig. 10.** Comparison between the end-shortening versus temperature paths from Correia and Rodrigues [55] anisothermal fire tests and shell finite element models for hot-rolled HEA section columns.

**Table 7**
Capacity predictions achieved using the proposed method and EN 1993-1-2 [1] compared with benchmark shell finite element model predictions for hot-rolled and welded steel columns at elevated temperatures analysed using the isothermal analysis method.

| Section | $\theta$ (°C) | N | $N_{Rd,\theta,shell}/N_{Rd,\theta,EC3}$ | | | | $N_{Rd,\theta,shell}/N_{Rd,\theta,prop}$ | | | |
|---|---|---|---|---|---|---|---|---|---|---|
| | | | Mean | CoV | Max | Min | Mean | CoV | Max | Min |
| I (hot-rolled) | | 324 | 1.27 | 0.271 | 2.12 | 0.82 | 1.08 | 0.045 | 1.24 | 0.93 |
| I (welded) | | 162 | 1.20 | 0.245 | 2.04 | 0.82 | 1.05 | 0.049 | 1.17 | 0.92 |
| SHS | 300,500,700 | 81 | 1.26 | 0.277 | 2.03 | 0.78 | 1.04 | 0.049 | 1.13 | 0.90 |
| RHS | | 162 | 1.25 | 0.256 | 2.01 | 0.83 | 1.05 | 0.045 | 1.21 | 0.93 |
| **Total** | | **729** | **1.25** | **0.264** | **2.12** | **0.78** | **1.06** | **0.048** | **1.24** | **0.90** |

limits fire design approach shown in Figs. 11–14, a distinction is made between the columns (i) for which the peak load governed and (ii) for those with more slender cross-sections where the strain limits were attained prior to the peak load. Typically, the peak load governs for the columns with low cross-section slendernesses $\bar{\lambda}_{p,\theta}$ and/or high member slendernesses $\bar{\lambda}_{\theta}$. Figs. 11–14 show that the proposed method provides very accurate and safe capacity predictions for I-section, SHS and RHS steel columns in fire.

In Table 7, the ratios of the ultimate resistance predictions obtained from the benchmark shell finite element models $N_{Rd,\theta,shell}$ to those determined using the proposed method $N_{Rd,\theta,prop}$ (i.e. $N_{Rd,\theta,shell}/N_{Rd,\theta,prop}$) are shown for all the considered hot-rolled and welded I-section, SHS and RHS steel columns analysed using the isothermal analysis technique; the ratios of the benchmark shell finite element model capacity predictions $N_{Rd,\theta,shell}$ to those determined through EN 1993-1-2 [1] $N_{Rd,\theta,EC3}$ (i.e. $N_{Rd,\theta,shell}/N_{Rd,\theta,EC3}$) are also displayed in the table. In the table, N refers to the number of considered columns. Comparing the average, coefficient of variation (CoV), maximum and minimum values of the $N_{Rd,\theta,shell}/N_{Rd,\theta,prop}$ and $N_{Rd,\theta,shell}/N_{Rd,\theta,EC3}$ ratios in Table 7, it is clear that the proposed method (i) results in significantly more accurate and consistent design predictions for steel columns at elevated temperatures compared to EN 1993-1-2 [1] and (ii) consistently yields safe-sided predictions for the capacity of steel columns analysed adopting the isothermal analysis method. In Fig. 15, the accuracy of the proposed design approach against that of the simplified calculation model of EN 1993-1-2 is also graphically illustrated, from which the significantly higher accuracy of the proposed method relative to EN 1993-1-2 [1] can also be observed.

*5.2. Members subjected to compression analysed using the anisothermal analysis method*

In this section, the accuracy of the proposed fire design approach is investigated for steel columns at elevated temperatures analysed adopting the anisothermal analysis method. Table 8 summarises the considered parameters. A total of 323 anisothermal analyses were performed considering (i) three cross-section types: I-sections, square and rectangular hollow sections (SHS & RHS); (ii) major and minor axis flexural buckling; (iii) the room temperature column slendernesses $\bar{\lambda}$ of 0.5, 1.0 and 1.5; (iv) the axial load intensities $\alpha_N$ of 0.25, 0.50 and 0.75 (i.e. $\alpha_N = N_{Ed}/N_{b,Rd} = 0.25$, 0.50 and 0.75 where $N_{b,Rd}$ is the room temperature column strength determined according to EN 1993-1-1 [20]); (v) axially and rotationally unrestrained columns; (vi) axially restrained columns with axial restraint ratios $\alpha_\Delta$ of 0.02, 0.05 and 0.10 (i.e. $\alpha_\Delta = k_\Delta/(EA_c/L) = 0.02$, 0.05 and 0.10) and (vii) axially and rotationally restrained columns with a rotational restraint ratio $\alpha_\varphi$ equal to 0.50 (i.e. $\alpha_\varphi = k_\varphi/(4EI_c/L) = 0.50$) and axial restraint ratios $\alpha_\Delta$ of 0.02, 0.05 and 0.10 (i.e. $\alpha_\Delta = k_\Delta/(EA_c/L) = 0.02$, 0.05 and 0.10). In the application of the proposed design approach, the temperatures of the columns were linearly increased in the second-order inelastic analyses of the beam finite element models. Axial restraint ratios $\alpha_\Delta = k_\Delta/(EA_c/L)$ and rotational restraint ratios $\alpha_\varphi = k_\varphi/(4EI_c/L)$ as well as the axial load intensities $\alpha_N = N_{Ed}/N_{b,Rd}$ were selected based on typical values used in previous studies [38,57]. Figs. 16 and 17 show comparisons of the limit temperatures obtained from the shell finite element models against those determined using the proposed fire design method for uniformly heated steel columns without and with axial and rotational end restraints respectively. Note that since shell finite element models are able to explicitly consider the influence of local buckling effects unlike beam finite element models used in the
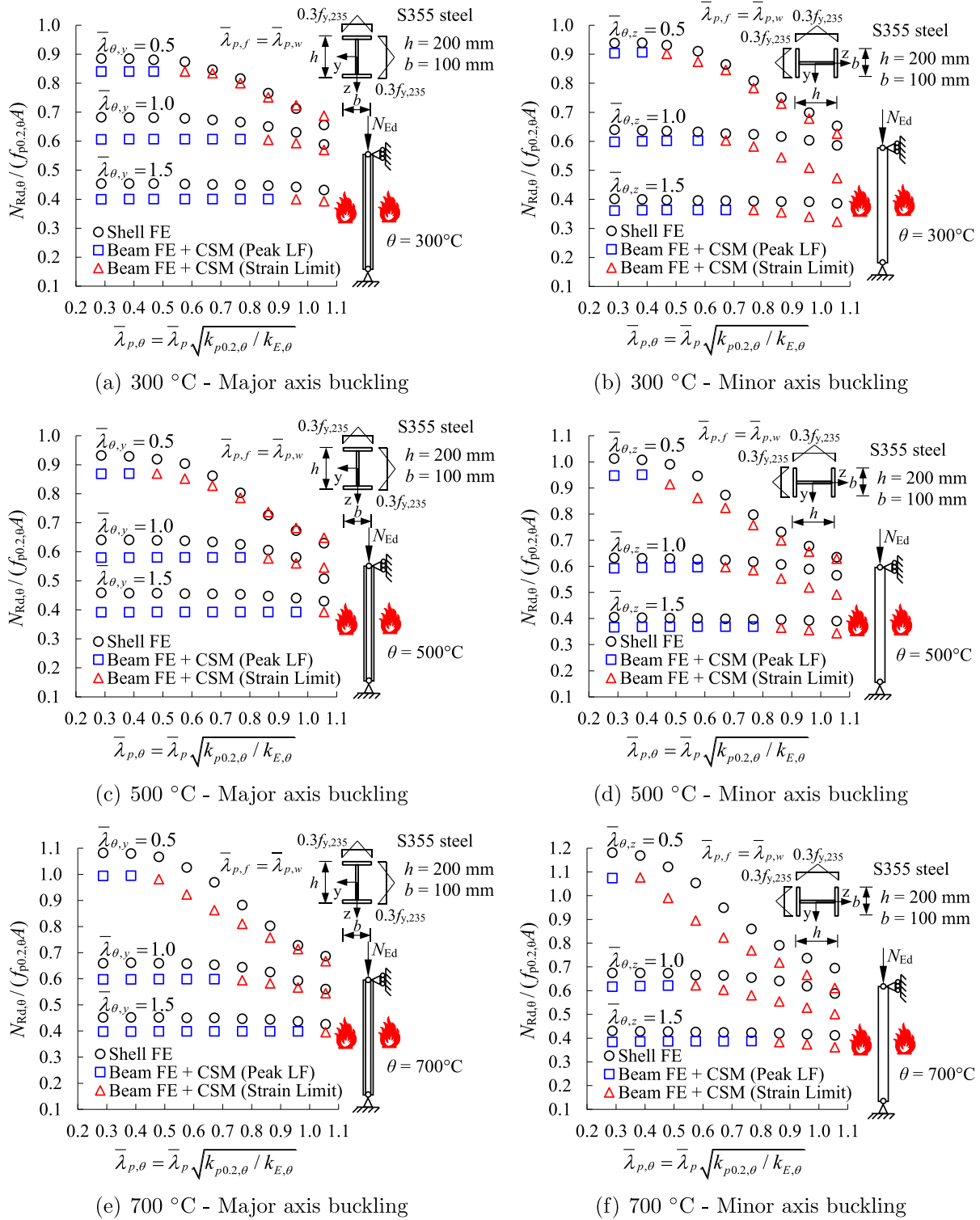
Fig. 11. Capacity predictions achieved using the proposed method and shell finite element models for hot-rolled I-section steel columns analysed adopting the isothermal analysis approach.

application of the proposed design approach, the critical temperatures at which the columns are no longer able to carry the applied loads are taken as the benchmark limit temperatures from the shell finite element models. As can be seen from Figs. 16 and 17, the limit temperature predictions obtained through the proposed method applied using the steps described in Section 3.5 agree well with the benchmark results obtained from the shell finite element models. Note that a range of $\alpha_N = N_{Ed}/N_{b,Rd}$ values are used in Figs. 16 and 17 in addition to the

$\alpha_N$ values considered in the parametric studies (see Table 8) to show the changes of the column limit temperatures $\theta_{Rd}$ with the change of the room temperature cross-section slendernesses $\bar{\lambda}_p$ of the columns.

Fig. 18 shows the development of the mechanical strain and internal axial force within a steel column which is fully fixed at both ends (i.e. fully restrained against translations and rotations) where only the temperature of the column is increased. The development of the maximum mechanical axial strain at the critical section derived in
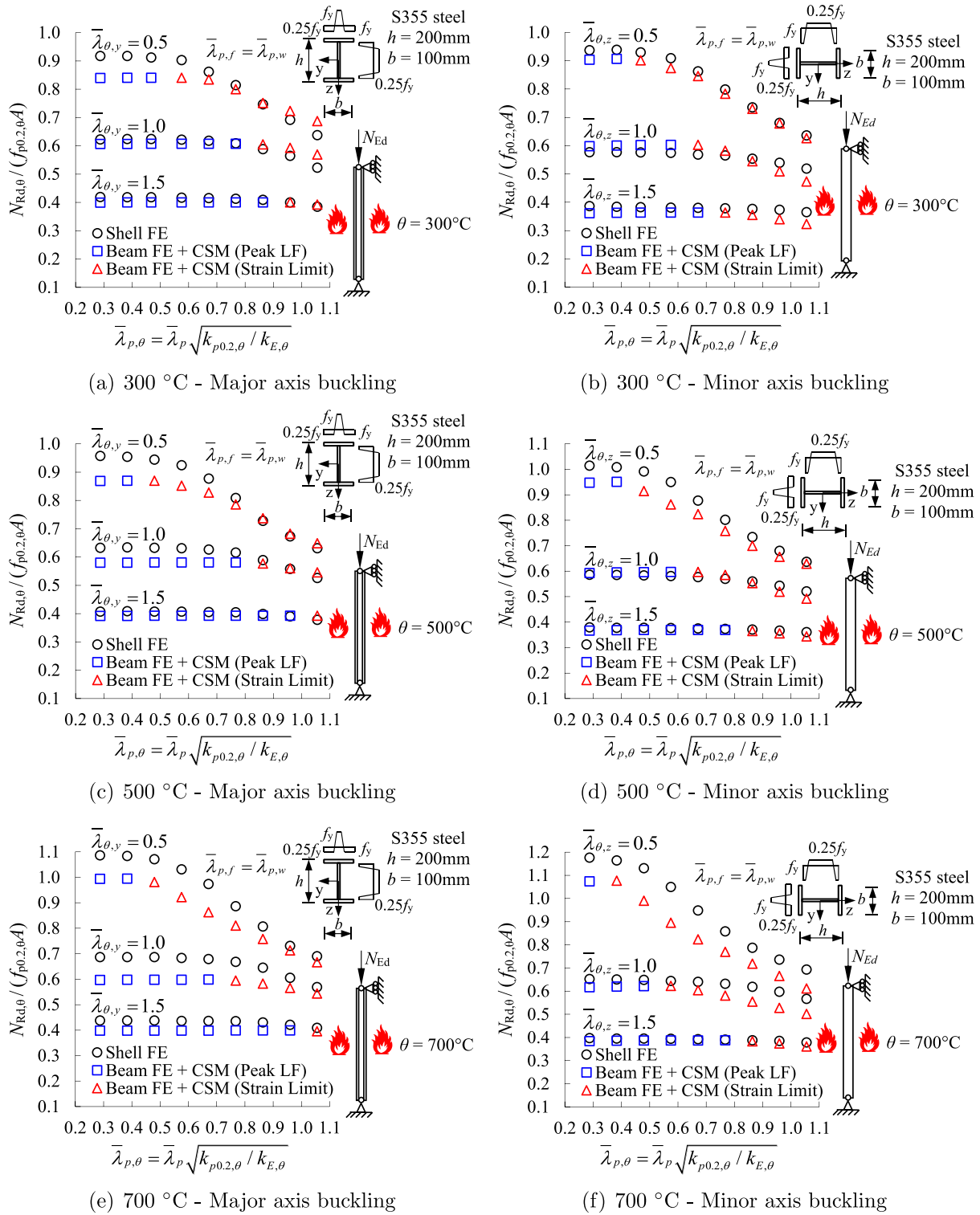
**Fig. 12.** Capacity predictions achieved using the proposed method and shell finite element models for welded I-section steel columns analysed adopting the isothermal analysis approach.

accordance with the proposed method using second-order inelastic beam finite element analysis is illustrated in Fig. 18(a) in conjunction with the temperature at which the strain limit specified according to the proposed method is attained $\theta_{csm}$, while Fig. 18(b) shows the development of the internal axial force within the column based on the analysis performed using the benchmark shell finite element model. Note that the critical cross-section is the cross-section where the maximum strain is observed in the column. It can be seen from Fig. 18 that

the temperature at which the strain limit is reached $\theta_{csm}$ corresponds well with the peak axial force in the column whereupon the local buckling occurs which was determined by means of the benchmark shell finite element model of the column. This further demonstrates the capability of the proposed method in predicting the local buckling temperatures within restrained columns. Note that in the fire design of steel columns with significantly high axial end-restraint stiffnesses by the proposed method, the critical temperature $\theta_{cr}$ at which the column
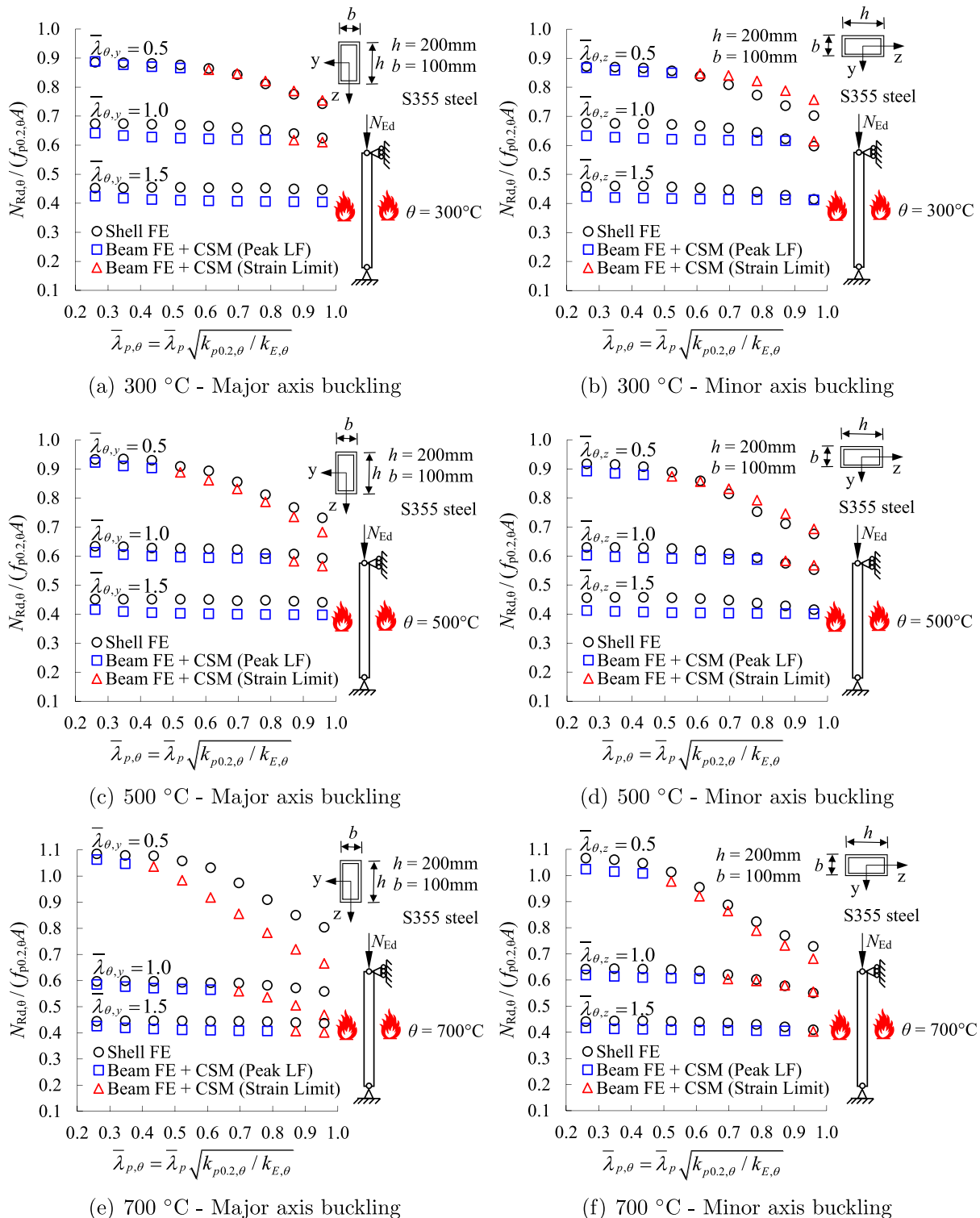
**Fig. 13.** Capacity predictions achieved using the proposed method and shell finite element models for hot-rolled steel RHS columns analysed adopting the isothermal analysis approach.

is no longer able to carry the applied load may occur at a higher temperature than the temperature at which the strain limit is achieved $\theta_{csm}$ (i.e. the local buckling temperature) due to the extensive post-buckling response; for such cases, the proposed method conservatively takes the limit temperature $\theta_{Rd}$ as the temperature at which the strain limit is attained $\theta_{csm}$ (i.e. the local buckling temperature). However, since the axial end-restraint stiffnesses are typically less than 10% of the axial stiffnesses of steel columns in realistic structures [38,58,59],

which has been covered in the parametric studies in this paper as shown in Table 8, the proposed fire design approach leads to quite accurate limit temperature $\theta_{Rd}$ predictions for restrained steel columns at elevated temperatures as shown in Fig. 17.

In Fig. 19(a), the axial displacement versus temperature response of the HE340AA column from the Dumont et al. [54] fire experiments described in Section 4.2 is compared against (i) the axial displacement
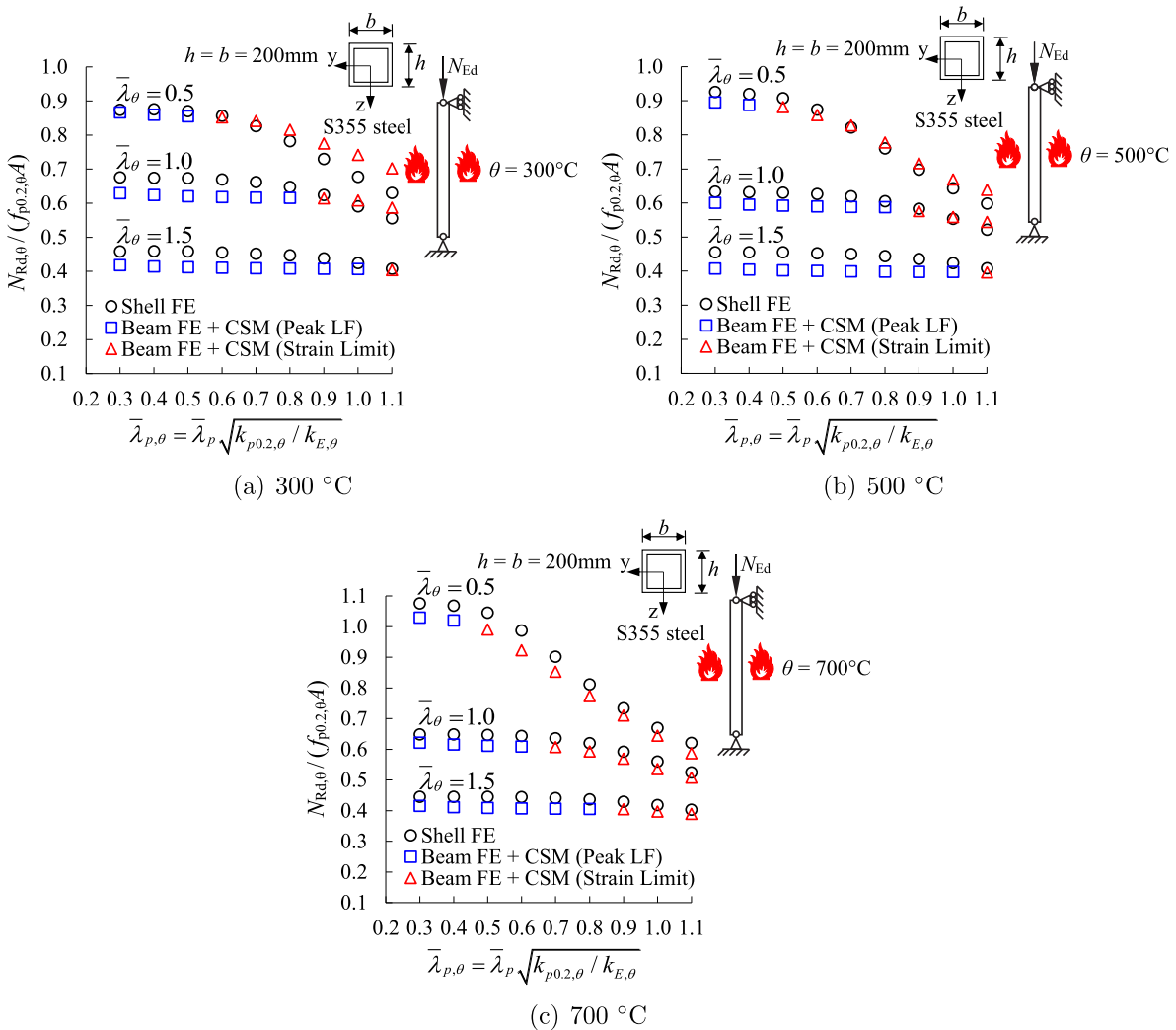
**Fig. 14.** Capacity predictions achieved using the proposed method and shell finite element models for hot-rolled steel SHS columns analysed adopting the isothermal analysis approach.
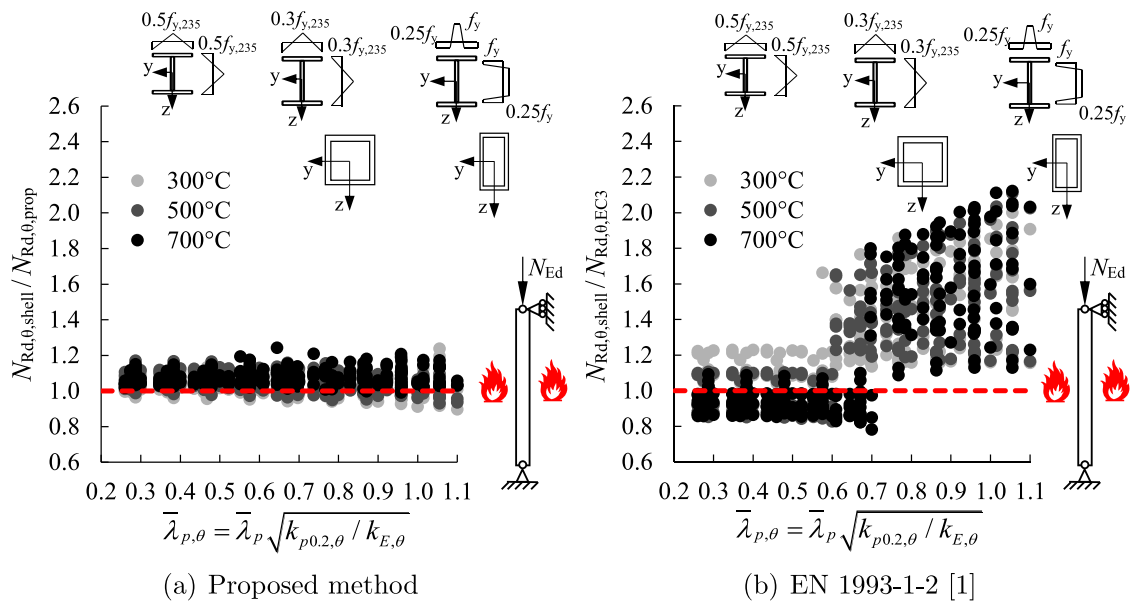


**Fig. 15.** Comparison of the accuracy of the proposed method against EN 1993-1-2 [1] for steel columns analysed adopting the isothermal analysis approach.

**Table 8**

Parameters used in the investigation of the accuracy of the proposed design approach for steel columns analysed adopting the anisothermal analysis approach.



| End restraint types & stiffnesses, cross-sections and loading conditions | Axial load intensity $\alpha_N$ | Member slenderness $\bar{\lambda}$ |
|---|---|---|
| *(column diagrams: Unrestrained, Axially restrained, Axially & rotationally restrained; Rolled I-sections; RHS; SHS)* | 0.25, 0.50, 0.75 | 0.5, 1.0, 1.5 |

**Table 9**

Comparison of the critical temperature predictions obtained through the proposed method and EN 1993-1-2 [1] against those determined through the benchmark shell finite element models for steel columns at elevated temperatures analysed adopting the anisothermal analysis technique.

| Section | Boundary conditions | N | $\theta_{Rd,shell}/\theta_{Rd,EC3}$ | | | | $\theta_{Rd,shell}/\theta_{Rd,prop}$ | | | |
|---|---|---|---|---|---|---|---|---|---|---|
| | | | Mean | CoV | Max | Min | Mean | CoV | Max | Min |
| I ($h/b = 1.0$) | Unrestrained | 24 | 1.15 | 0.190 | 1.68 | 0.89 | 1.08 | 0.109 | 1.43 | 0.99 |
| | Axially restrained | 64 | 0.90 | 0.228 | 1.48 | 0.46 | 1.07 | 0.066 | 1.27 | 0.97 |
| | Axially & Rotationally restrained | 64 | 1.15 | 0.182 | 1.65 | 0.87 | 1.13 | 0.126 | 1.78 | 1.01 |
| I ($h/b = 2.0$) | Unrestrained | 24 | 1.24 | 0.221 | 1.82 | 0.88 | 1.10 | 0.109 | 1.41 | 1.00 |
| | Axially restrained | 54 | 0.96 | 0.222 | 1.48 | 0.57 | 1.11 | 0.102 | 1.62 | 1.01 |
| | Axially & Rotationally restrained | 54 | 1.25 | 0.203 | 1.65 | 0.71 | 1.13 | 0.132 | 1.81 | 0.99 |
| SHS | Unrestrained | 15 | 0.95 | 0.102 | 1.20 | 0.78 | 1.05 | 0.051 | 1.16 | 0.92 |
| RHS | Unrestrained | 24 | 0.95 | 0.116 | 1.15 | 0.61 | 1.04 | 0.048 | 1.17 | 0.94 |
| **Total** | | **323** | **1.08** | **0.239** | **1.82** | **0.46** | **1.10** | **0.109** | **1.81** | **0.92** |

**Table 10**

Reliability of the proposed method and EN 1993-1-2 [1] for the assessment of steel columns in fire on the basis of the reliability criteria defined by Kruppa [56].

| | Analysis type | Criterion 1 | Criterion 2 | Criterion 3 |
|---|---|---|---|---|
| Proposed design method | Isothermal | 0.00 | 9.74 | −5.54 |
| | Anisothermal | 0.00 | 2.17 | −8.16 |
| EN 1993-1-2 [1] | Isothermal | 6.31[a] | 33.88[a] | −14.53 |
| | Anisothermal | 16.72[a] | 44.89[a] | −1.69 |

[a]Indicates the corresponding criterion has been violated.

versus temperature response determined through the proposed approach using second-order inelastic analysis with beam finite elements and (ii) the numerical axial displacement versus temperature response determined in [54] for the tested Class 4 HE340AA steel column. Note that the numerical axial deformation versus temperature response was determined in [54] using the computer software SAFIR [41] where shell finite elements were employed to create the numerical model. According to the proposed method, the failure occurs at a temperature of 620.96 °C when the strain limit is attained as shown in Fig. 19(b) (i.e. $\theta_{Rd} = \theta_{csm} = 620.96$ °C). As shown in Fig. 19(a), the failure temperatures obtained from the physical experiment $\theta_{test}$ and shell finite element model $\theta_{shell}$ of Dumont et al. [54] are 623.81 °C and 631.44 °C, respectively (i.e. $\theta_{test} = 623.81$ °C and $\theta_{shell} = 631.44$ °C). The good agreement between the limit temperature $\theta_{Rd}$ determined through the proposed method and the experimental $\theta_{test}$ and numerical

$\theta_{shell}$ failure temperatures shown in Fig. 19(a) from Dumont et al. [54] further verify the accuracy of the proposed fire design approach in predicting the structural response of steel columns in fire.

Table 9 illustrates the ratios of the limit temperatures from the shell finite element models $\theta_{Rd,shell}$ to those achieved using the proposed design method $\theta_{Rd,prop}$ (i.e. $\theta_{Rd,shell}/\theta_{Rd,prop}$) and EN 1993-1-2 [1] $\theta_{Rd,EC3}$ (i.e. $\theta_{Rd,shell}/\theta_{Rd,EC3}$) for uniformly heated steel columns with and without axial and rotational end restraints. Fig. 20 also shows the ratios of the limit temperature predictions from the shell finite element models $\theta_{Rd,shell}$ to those achieved using the proposed design method $\theta_{Rd,prop}$ (i.e. $\theta_{Rd,shell}/\theta_{Rd,prop}$) and EN 1993-1-2 [1] $\theta_{Rd,EC3}$ (i.e. $\theta_{Rd,shell}/\theta_{Rd,EC3}$) for all the considered steel columns analysed through the anisothermal analysis technique. Note that in the determination of the limit temperatures through EN 1993-1-2 [1] $\theta_{Rd,EC3}$, an iterative approach was adopted by calculating the column strengths at different temperature values through the formulae provided in Section 2; the temperature value providing the ultimate column resistance $N_{b,fi,Rd}$ equal to the applied axial load $N_{Ed}$ (i.e. $N_{b,fi,Rd} = N_{Ed}$) was assumed as the critical temperature according to EN 1993-1-2 [1] $\theta_{Rd,EC3}$. The $\theta_{Rd,shell}/\theta_{Rd,prop}$ and $\theta_{Rd,shell}/\theta_{Rd,EC3}$ ratios in Table 9 and Fig. 20 verify that the proposed method provides safe capacity predictions for the columns analysed using the anisothermal approach which are both more accurate and consistent than the EN 1993-1-2 [1] design predictions. Moreover, the results demonstrate that the proposed method is capable of predicting the behaviour of columns with complex conditions such as end-restraints which are typically neglected in the simplified calculation model of EN 1993-1-2 [1].
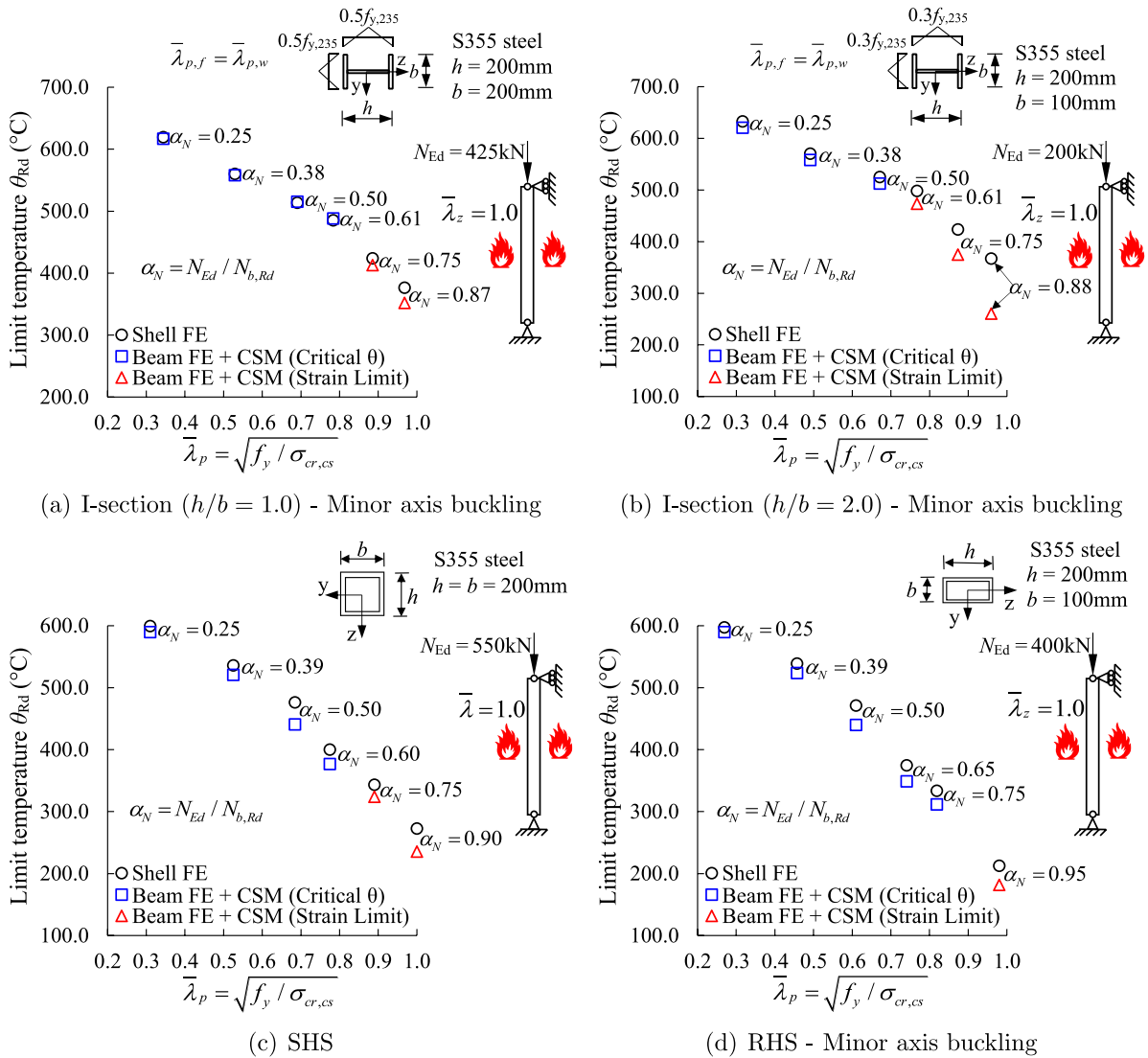
**Fig. 16.** Capacity predictions of the proposed method and benchmark shell finite element models for steel columns analysed adopting the anisothermal analysis technique.

## 5.3. Reliability analysis

The reliability of the proposed design method and that of the EN 1993-1-2 [1] simplified calculation model for the fire design of steel columns is assessed in Table 10 adopting the three reliability criteria proposed by Kruppa [56] for the methods developed for the fire design of steel elements. Note that in the table, the reliability of the proposed method and the simplified calculation model of EN 1993-1-2 [1] is assessed for the isothermal and anisothermal analysis techniques separately, considering all the parameters taken into account in the numerical parametric studies as set out in Sections 5.1 and 5.2. Criterion 1 of Kruppa [56] states that none of the capacity predictions of a design method $R_{method}$ should exceed the predictions achieved using the GMNIA of finite element models $R_{GMNIA}$ by more than 15% (i.e. $(R_{method} - R_{GMNIA})/R_{GMNIA} \leq 15\%$). Criterion 2 of Kruppa [56] states that less than 20% of the design predictions should be on the unsafe side (i.e. $num(R_{method} > R_{GMNIA})/num(R_{GMNIA}) \leq 20\%$). Finally, Criterion 3 of Kruppa [56] states that the design predictions should be safe-sided on average (i.e. $\overline{X}[(R_{method} - R_{GMNIA})/R_{GMNIA}] \leq 0\%$). In Table 10, the percentage of design predictions $R_{method}$ exceeding GMNIA predictions $R_{GMNIA}$ by more than 15% are shown under Criterion 1, the percentage of unsafe design predictions (i.e. $R_{method} > R_{GMNIA}$) are shown under Criterion 2 and the average percentage differences between the GMNIA predictions $R_{GMNIA}$ and design predictions $R_{method}$ are shown

under Criterion 3 where negative percentages indicate that the design capacity predictions are safe-sided on average. Table 10 shows that the proposed method fulfils all the three reliability criteria of Kruppa [56]. On the other hand, the simplified calculation model of EN 1993-1-2 [1] fails to satisfy Criterion 1 and Criterion 2 when the isothermal or anisothermal analysis technique is adopted, thus indicating that the proposed method leads to a higher level of reliability relative to the simplified calculation model of EN 1993-1-2 [1] in the fire design of steel columns.

## 6. Summary of the proposed design method using worked examples

In this section the application of the proposed design method is summarised using two worked examples. Worked example 1 considers a column in fire analysed using the isothermal analysis approach. Worked example 2 considers a restrained column in fire analysed using the anisothermal analysis approach.

### 6.1. Worked example 1

Worked example 1 summarised in Fig. 21 considers an S355 steel ($f_y = 355$ N/mm$^2$) RHS 200 × 100 × 6 column subjected to a design axial load $N_{Ed}$ of 500 kN (i.e. $N_{Ed} = 500$ kN) at 500 °C. The column is analysed using the isothermal analysis approach.
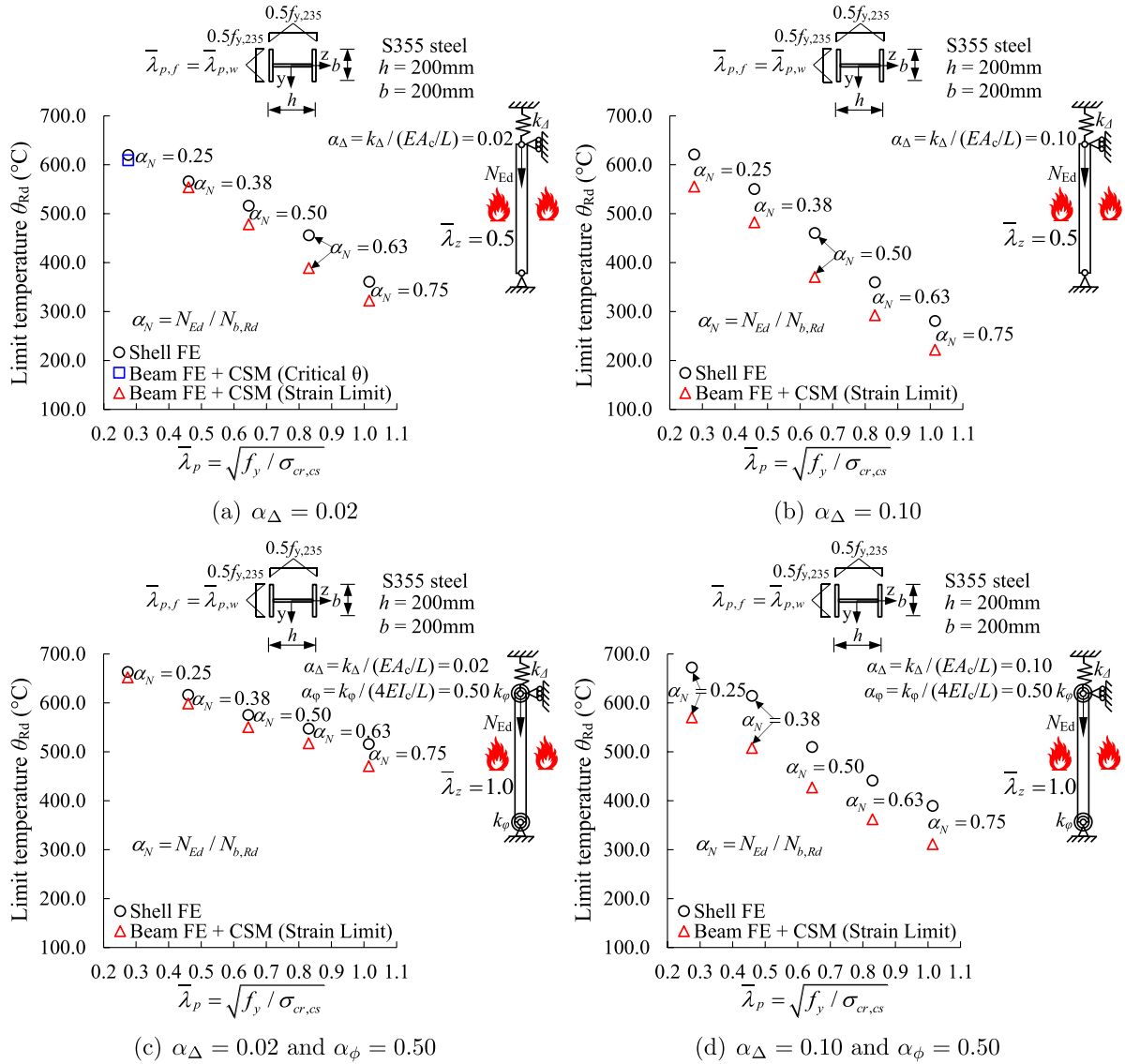
**Fig. 17.** Capacity predictions of the proposed method and benchmark shell finite element models for restrained steel I-section columns analysed adopting the anisothermal analysis technique.
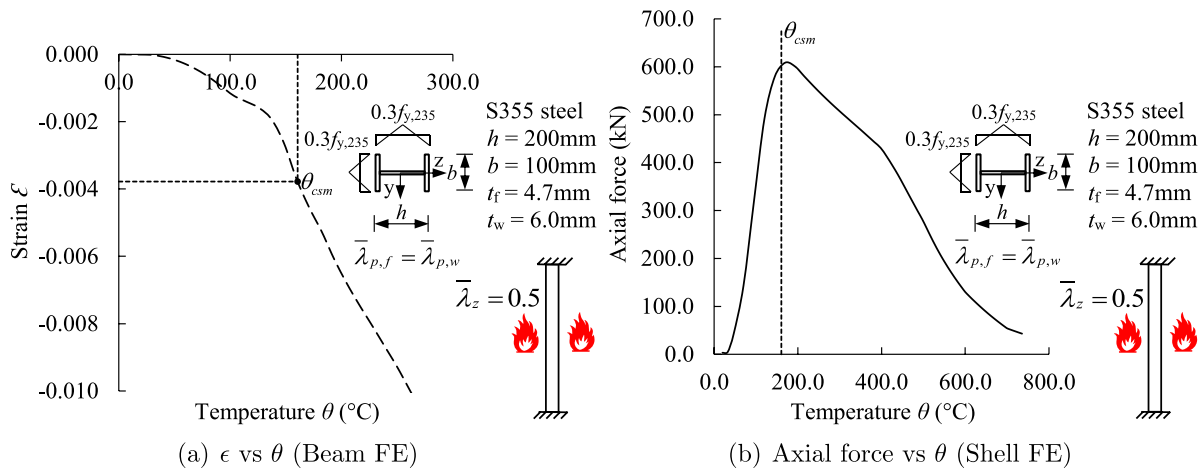


**Fig. 18.** Maximum mechanical strain at the critical cross-section and internal axial force plotted against temperature for a steel I-section column fully restrained against all translations and rotations at both ends. Note that the critical cross-section is the cross-section where the maximum mechanical strain is observed in the column.
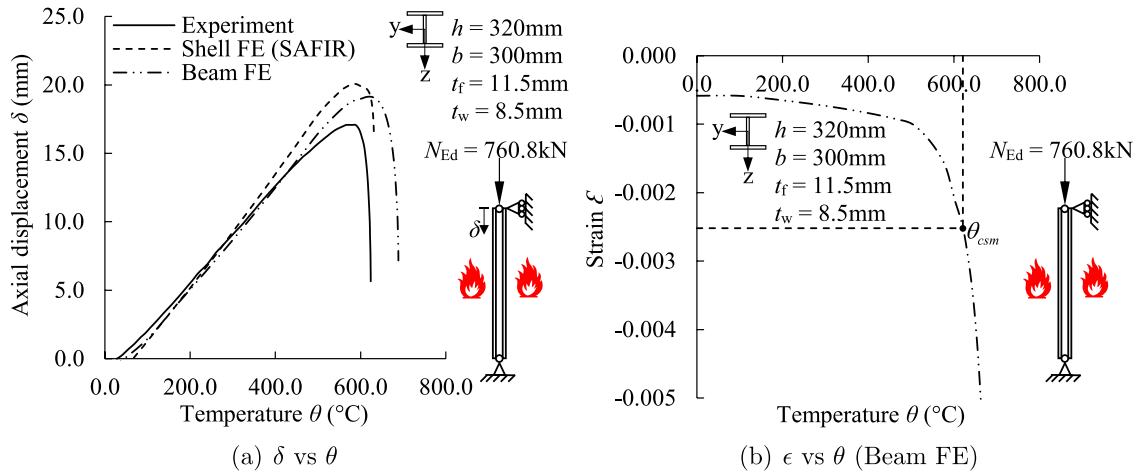
(a) $\delta$ vs $\theta$

(b) $\epsilon$ vs $\theta$ (Beam FE)

**Fig. 19.** Axial displacement and maximum mechanical strain at the critical cross-section plotted against temperature for the HE340AA column from the Dumont et al. [54] tests. Note that the critical cross-section is the cross-section where the maximum mechanical strain is observed in the column.
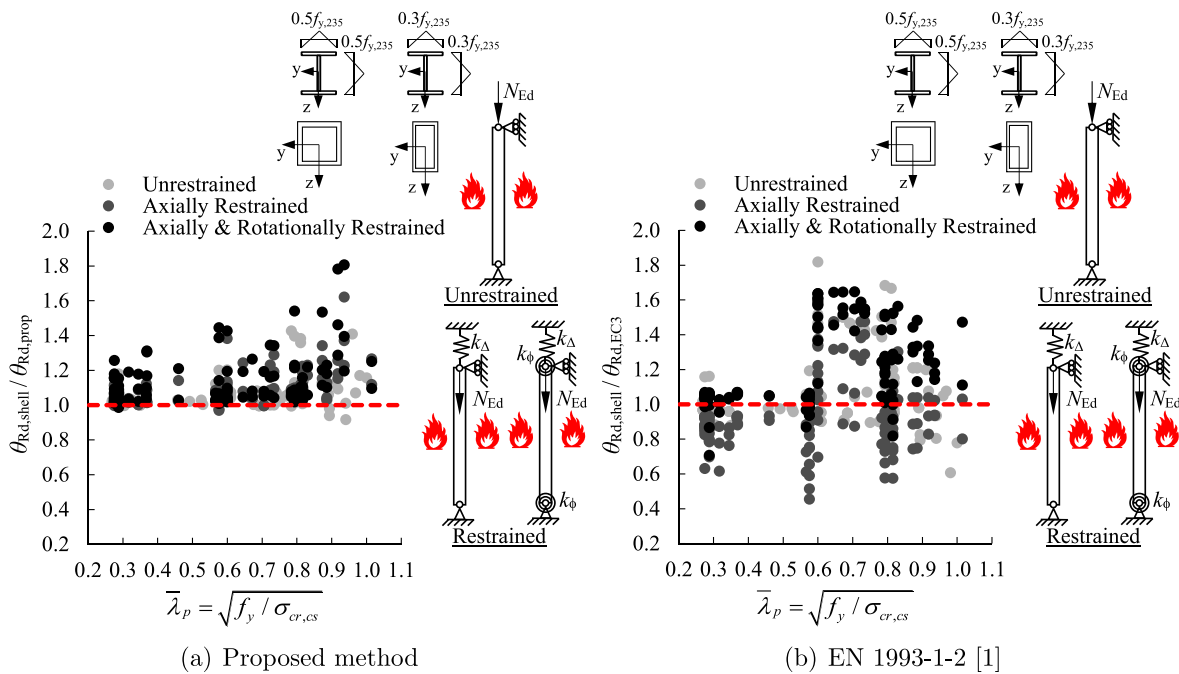




(a) Proposed method

(b) EN 1993-1-2 [1]

**Fig. 20.** Comparison of the accuracy of the proposed method against EN 1993-1-2 [1] for steel columns analysed adopting the anisothermal analysis technique.
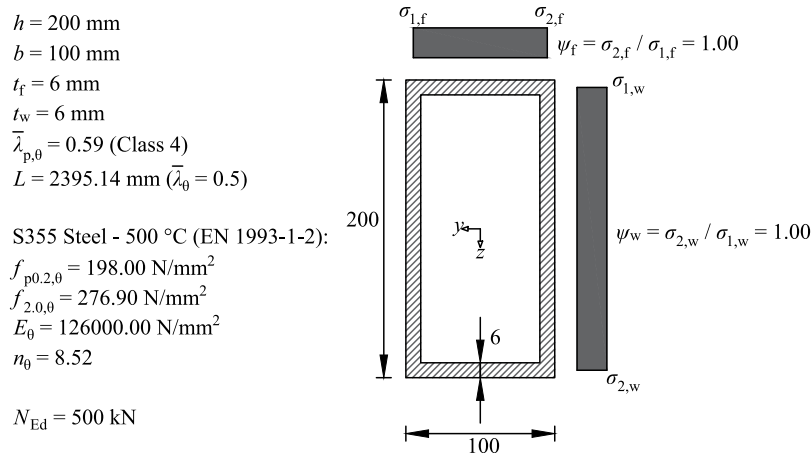


$h = 200$ mm
$b = 100$ mm
$t_f = 6$ mm
$t_w = 6$ mm
$\overline{\lambda}_{p,\theta} = 0.59$ (Class 4)
$L = 2395.14$ mm ($\overline{\lambda}_\theta = 0.5$)

S355 Steel - 500 °C (EN 1993-1-2):
$f_{p0.2,\theta} = 198.00$ N/mm$^2$
$f_{2.0,\theta} = 276.90$ N/mm$^2$
$E_\theta = 126000.00$ N/mm$^2$
$n_\theta = 8.52$

$N_{Ed} = 500$ kN

**Fig. 21.** Worked example 1: RHS 200 × 100 × 6 column subjected to compression (major axis buckling) at 500 °C. All dimensions are in mm. Not to scale.

### 6.1.1. Calculation of the full cross-section elastic local buckling stress $\sigma_{cr,cs}$

The method put forward in [22] is used in this section to calculate $\sigma_{cr,cs}$. The plate buckling coefficients for isolated internal flange plates with simply-supported $k_f^{SS}$ and fixed $k_f^F$ boundary conditions are 4.00 and 6.97 respectively (i.e. $k_f^{SS} = 4.00$ and $k_f^F = 6.97$), and the plate buckling coefficients for isolated internal web plates with simply-supported $k_w^{SS}$ and fixed $k_w^F$ boundary conditions are 4.00 and 6.97 respectively (i.e. $k_w^{SS} = 4.00$ and $k_w^F = 6.97$). The corresponding elastic buckling stresses with simply-supported boundary conditions $\sigma_{cr}^{SS}$ are 3093.17 MPa for the flange (i.e. $\sigma_{cr,f}^{SS} = 3093.17$ MPa) and 726.20 MPa for the web (i.e. $\sigma_{cr,w}^{SS} = 726.20$ MPa); and the elastic buckling stresses with fixed boundary conditions $\sigma_{cr}^F$ are 5389.84 MPa for the flange (i.e. $\sigma_{cr,f}^F = 5389.84$ MPa) and 1265.40 MPa for the web (i.e. $\sigma_{cr,w}^F = 1265.40$ MPa). Since the column is subjected to pure compression, both the flange load correction factor $\beta_f$ and the web load correction factor $\beta_w$ are equal to one (i.e. $\beta_f = 1$ and $\beta_w = 1$). The governing ratio $\phi$ is calculated as:

$$\phi = \frac{\beta_f \sigma_{cr,f}^{SS}}{\beta_w \sigma_{cr,w}^{SS}} = 4.26$$

Since $\phi > 1$, the web plate is deemed critical. The lower and upper bounds to the full cross-section local buckling stress are as follows:

$$\sigma_{cr,p}^{SS} = min\left(\beta_f \sigma_{cr,f}^{SS}, \beta_w \sigma_{cr,w}^{SS}\right) = 726.20 \text{ MPa}$$

$$\sigma_{cr,p}^F = min\left(\beta_f \sigma_{cr,f}^F, \beta_w \sigma_{cr,w}^F\right) = 1265.40 \text{ MPa}$$

The interaction coefficient $\xi$ for a RHS subjected to compression with major axis buckling is given by:

$$\xi = \frac{t_f}{t_w}\left(0.53 - \frac{\alpha_w}{\phi}\right) = 0.429$$

where the coefficient $\alpha_w = 0.63 - 0.1(h/b) \leq 0.53$. The full cross-section elastic local buckling stress $\sigma_{cr,cs}$ is then calculated as:

$$\sigma_{cr,cs} = \sigma_{cr,p}^{SS} + \xi(\sigma_{cr,p}^F - \sigma_{cr,p}^{SS}) = 726.20 + 0.429(1265.40 - 726.20)$$
$$= 957.54 \text{ MPa}$$

It should be noted that the finite strip analysis software CUFSM [23] could also be used to determine the full cross-section local buckling stress $\sigma_{cr,cs}$, which would result in $\sigma_{cr,cs}$ being equal to 989.95 MPa for the considered cross-section and loading type.

### 6.1.2. Calculation of the elevated temperature cross-section slenderness $\overline{\lambda}_{p,\theta}$

The elevated temperature cross-section slenderness $\overline{\lambda}_{p,\theta}$ is calculated using the room temperature cross-section slenderness $\overline{\lambda}_p$, the 0.2% proof strength reduction factor $k_{p0.2,\theta}$ equal to 0.56 at 500 °C (i.e. $k_{p0.2,\theta} = 0.56$) and the elastic modulus reduction factor $k_{E,\theta}$ equal to 0.60 at 500 °C (i.e. $k_{E,\theta} = 0.60$).

$$\overline{\lambda}_{p,\theta} = \overline{\lambda}_p \sqrt{\frac{k_{p0.2,\theta}}{k_{E,\theta}}} = \sqrt{\frac{f_y}{\sigma_{cr,cs}}} \sqrt{\frac{k_{p0.2,\theta}}{k_{E,\theta}}} = \sqrt{\frac{355.00}{957.54}} \sqrt{\frac{0.56}{0.60}} = 0.59$$

### 6.1.3. Calculation of the elevated temperature CSM strain limit $\epsilon_{csm,\theta}$

$\epsilon_{csm,\theta}$ is determined using the elevated temperature base curve shown in Fig. 3. Since $\overline{\lambda}_{p,\theta} < 0.68$, the cross-section is considered non-slender and therefore $\epsilon_{csm,\theta}/\epsilon_{y,\theta}$ is given as:

$$\frac{\epsilon_{csm,\theta}}{\epsilon_{y,\theta}} = \frac{0.25}{\overline{\lambda}_{p,\theta}^{3.6}} + \frac{0.002}{\epsilon_{y,\theta}} \leq \left(\Omega, \frac{C_1}{\epsilon_{y,\theta}}\right) = 2.97$$

which is smaller than the upper limit $\Omega$ set to 15 (i.e. $\Omega = 15$) and the upper limit $C_1/\epsilon_{y,\theta}$ equal to $0.02/\epsilon_{y,\theta}$ (i.e. $C_1 = 0.02/\epsilon_{y,\theta}$). The elevated temperature yield strain $\epsilon_{y,\theta}$ is equal to 0.00157 (i.e. $\epsilon_{y,\theta} = 0.00157$). Thus, $\epsilon_{csm,\theta}$ is then calculated as:

$$\epsilon_{csm,\theta} = 2.97\epsilon_{y,\theta} = 2.97 \times 0.00157 = 0.0047$$

### 6.1.4. GMNIA using beam finite elements adopting the isothermal approach

Second-order inelastic analysis is performed using 101 beam finite elements to discretise the column over its 2395.14 mm length. The model uses equivalent geometric imperfections with a magnitude equal to:

$$e_0 = \alpha\beta L \geq L/1000 = 0.53 \times (1/250) \times 2395.14 \geq 2395.14/1000 = 5.07 \text{ mm}$$

where the imperfection factor $\alpha$ is calculated as $0.65\sqrt{235/f_y}$ and the reference bow imperfection $\beta$ is equal to 1/250 (i.e. $\beta = 1/250$). The EN 1993-1-2 [1] elevated temperature material model is used in the analysis. The analysis is performed by first increasing the temperature of the column to 500 °C followed by the application of an incrementally increasing axial load using the modified Riks method. Fig. 22 shows the applied load versus the maximum mechanical strain at the critical cross-section. As can be seen in Fig. 22, the strain limit is obtained at a load $F_{csm,\theta}$ of 583.60 kN prior to the peak load $F_{peak,\theta}$ of 602.11 kN; thus, the capacity of the column is governed by the strain limit.

### 6.1.5. Resistance verification against applied load

The characteristic value of the resistance of the column is equal to the load at which the critical strain in a cross-section reaches the strain limit. The design value of this resistance $N_{Rd,\theta}$ is attained by dividing the load at which the strain limit is attained $F_{csm,\theta}$ by the partial factor for resistance in fire conditions $\gamma_{M,fi}$ equal to 1.00 (i.e. $\gamma_{M,fi} = 1.00$), thus the design resistance is given by:

$$N_{Rd,\theta} = \frac{F_{csm,\theta}}{\gamma_{M,fi}} = \frac{583.60}{1.00} = 583.60 \text{ kN}$$

Comparing this to the applied design axial load $N_{Ed}$ of 500 kN:

$$\frac{N_{Ed}}{N_{Rd,\theta}} = \frac{500.00}{583.60} = 0.86 \leq 1.00 \quad \therefore \text{Pass}$$

Therefore, the column is deemed satisfactory at 500 °C.

### 6.2. Worked example 2

Worked example 2 shown in Fig. 23 considers a grade S355 steel ($f_y = 355$ N/mm$^2$) HEAA 300 column subjected to a design axial load $N_{Ed}$ of 530 kN (i.e. $N_{Ed} = 530$ kN) and required to withstand fire with a design temperature $\theta_{Ed}$ of 450 °C. The column is analysed anisothermally and has axial end-restraint $k_\Delta$ equivalent to 36.47 kN/mm (i.e. $k_\Delta = 36.47$ kN/mm) where $k_\Delta$ is equal to the axial restraint stiffness ratio $\alpha_\Delta = 0.1$ multiplied by the axial stiffness of the column $k_{\Delta,c}$ (i.e. $k_\Delta = \alpha_\Delta k_{\Delta,c} = 0.1k_{\Delta,c}$). In addition, the column has rotational end-restraints $k_\varphi$ equal to 11 318.46 kNm/rad (i.e. $k_\varphi = 11318.46$ kNm/rad) where $k_\varphi$ is equal to the rotational restraint stiffness ratio $\alpha_\varphi = 0.5$ multiplied by the rotational stiffness of the column $k_{\varphi,c}$ (i.e. $k_\varphi = \alpha_\varphi k_{\varphi,c} = 0.5k_{\varphi,c}$).

### 6.2.1. Calculation of the full cross-section elastic local buckling stress $\sigma_{cr,cs}$

The procedure defined in [22] is used in this section to calculate $\sigma_{cr,cs}$. The plate buckling coefficients for isolated outstand flange plates with simply-supported $k_f^{SS}$ and fixed $k_f^F$ boundary conditions are 0.43 and 1.25 respectively (i.e. $k_f^{SS} = 0.43$ and $k_f^F = 1.25$), and the plate buckling coefficients for isolated internal web plates with simply-supported $k_w^{SS}$ and fixed $k_w^F$ boundary conditions are 4.00 and 6.97 respectively (i.e. $k_w^{SS} = 4.00$ and $k_w^F = 6.97$). The corresponding elastic buckling stresses with simply-supported boundary conditions $\sigma_{cr}^{SS}$ are 399.91 MPa for the flange (i.e. $\sigma_{cr,f}^{SS} = 399.91$ MPa) and 575.10 MPa for the web (i.e. $\sigma_{cr,w}^{SS} = 575.10$ MPa); and the elastic buckling stresses with fixed boundary conditions $\sigma_{cr}^F$ are 1162.53 MPa for the flange (i.e. $\sigma_{cr,f}^F = 1162.53$ MPa) and 1002.12 MPa for the web (i.e. $\sigma_{cr,w}^F = 1002.12$ MPa). Since the column is subjected to pure compression, both the flange load correction factor $\beta_f$ and the web load correction factor
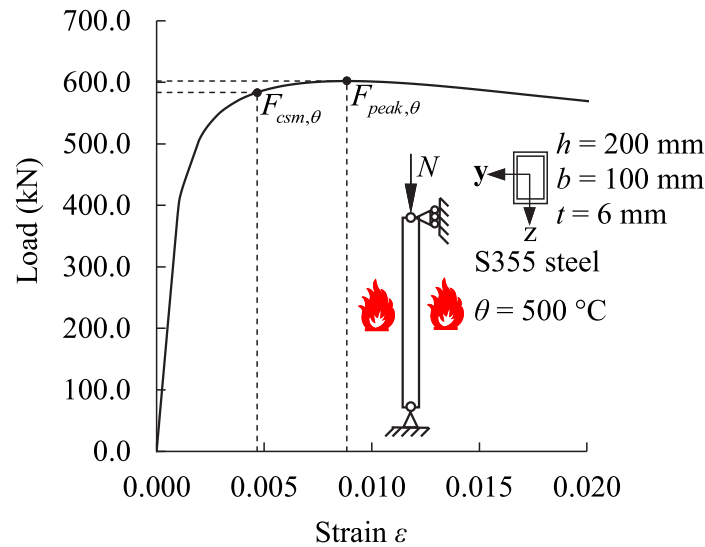
**Fig. 22.** Applied axial load versus the maximum mechanical strain at the critical cross-section of the RHS column. Note that the critical cross-section is the cross-section where the maximum mechanical strain is observed in the column.
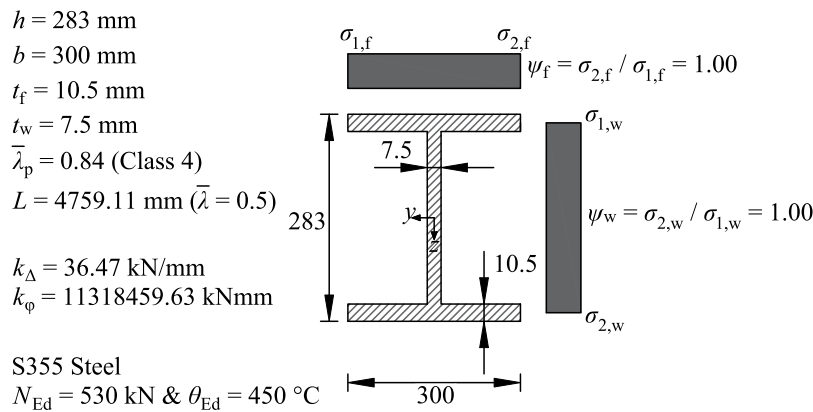


**Fig. 23.** Worked example 2: HEAA 300 column subjected to compression (major axis buckling). All dimensions are in mm. Not to scale.

$\beta_w$ are equal to one (i.e. $\beta_f = 1$ and $\beta_w = 1$). The governing ratio $\phi$ is calculated as:

$$\phi = \frac{\beta_f \sigma_{cr,f}^{SS}}{\beta_w \sigma_{cr,w}^{SS}} = 0.70$$

Since $\phi < 1$, the flange plate is deemed critical. The lower and upper bounds to the full cross-section local buckling stress are as follows:

$$\sigma_{cr,p}^{SS} = min\left(\beta_f \sigma_{cr,f}^{SS}, \beta_w \sigma_{cr,w}^{SS}\right) = 399.91 \text{ MPa}$$

$$\sigma_{cr,p}^{F} = min\left(\beta_f \sigma_{cr,f}^{F}, \beta_w \sigma_{cr,w}^{F}\right) = 1002.12 \text{ MPa}$$

The interaction coefficient $\xi$ for an I-section subjected to compression with major axis buckling is given by:

$$\xi = 0.15\frac{t_f}{t_w}\phi \geq \frac{t_w}{t_f}(0.4 - 0.25\phi) = 0.162$$

The full cross-section elastic local buckling stress $\sigma_{cr,cs}$ is then calculated as:

$$\sigma_{cr,cs} = \sigma_{cr,p}^{SS} + \xi(\sigma_{cr,p}^{F} - \sigma_{cr,p}^{SS}) = 399.91 + 0.162(1002.12 - 399.91)$$

$$= 497.19 \text{ MPa}$$

Note that the full cross-section local buckling stress $\sigma_{cr,cs}$ determined using the finite strip analysis software CUFSM [23] is equal to 519.22 MPa for the considered cross-section and loading type.

*6.2.2. GMNIA using beam finite elements adopting the anisothermal approach*

Second-order inelastic analysis is performed using 101 beam finite elements to discretise the column over its 4759.11 mm length. The model uses equivalent geometric imperfections with a magnitude equal to:

$$e_0 = \alpha\beta L \geq L/1000 = 0.53 \times (1/250) \times 4759.11 \geq 4759.11/1000$$

$$= 10.07 \text{ mm}$$

where the imperfection factor $\alpha$ is calculated as $0.65\sqrt{235/f_y}$ and the reference bow imperfection $\beta$ is equal to 1/250 (i.e. $\beta = 1/250$). The EN 1993-1-2 [1] elevated temperature material model is used during the analysis and translational and rotational springs are utilised to model the axial and rotational end-restraints. The analysis is performed by first increasing the axial load $N_{Ed}$ to 530 kN followed by the application of an incrementally increasing temperature using a uniform temperature distribution. The elevated temperature cross-section slenderness $\bar{\lambda}_{p,\theta}$ is calculated at each temperature increment as follows:

$$\bar{\lambda}_{p,\theta} = \sqrt{\frac{f_y}{\sigma_{cr,cs}}}\sqrt{\frac{k_{p0.2,\theta}}{k_{E,\theta}}}$$

where $k_{p0.2,\theta}$ is the 0.2% proof strength reduction factor and $k_{E,\theta}$ is the elastic modulus reduction factor. In addition, $\epsilon_{csm,\theta}$ is determined at each temperature increment using the elevated temperature base curve shown in Fig. 3. The calculated elevated temperature cross-section
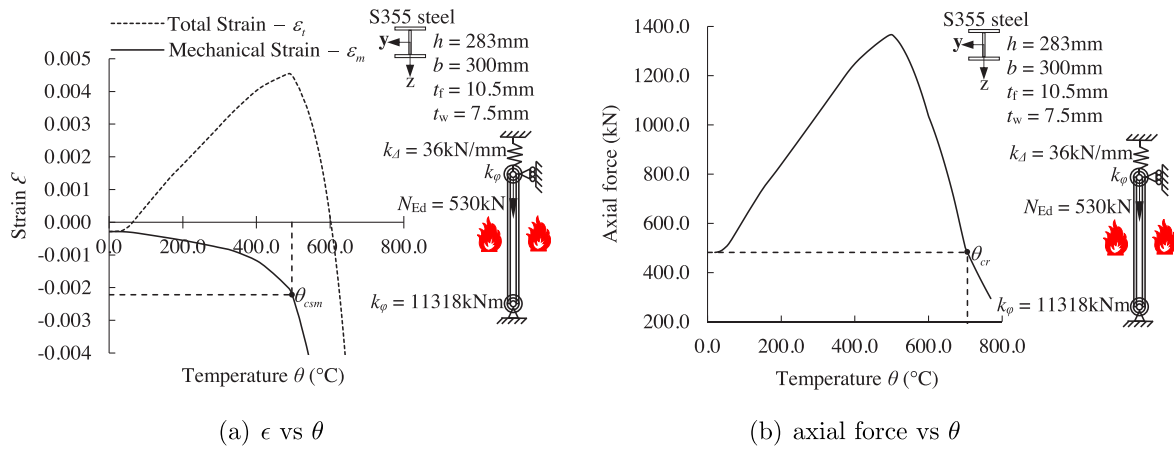
(a) $\epsilon$ vs $\theta$



(b) axial force vs $\theta$

**Fig. 24.** Total strain and maximum mechanical strain at the critical cross-section and internal axial force plotted against temperature for the HEAA 300 restrained column derived by conducting anisothermal analysis. Note that the critical cross-section is the cross-section where the maximum mechanical strain is observed in the column and the total strain shown in the figure is measured at the point where the maximum mechanical strain is observed.

slendernesses $\overline{\lambda}_{p,\theta}$ of the column cross-section are greater than 0.68 (i.e. $\overline{\lambda}_{p,\theta} > 0.68$); thus, the column cross-section is considered slender and $\epsilon_{csm,\theta}/\epsilon_{y,\theta}$ is determined at each temperature increment as:

$$\epsilon_{csm,\theta}/\epsilon_{y,\theta} = \left(1 - \frac{0.222}{\overline{\lambda}_{p,\theta}^{-1.05}}\right)\frac{1}{\overline{\lambda}_{p,\theta}^{-1.05}} + \frac{0.002(\sigma/f_{p0.2,\theta})^{n_\theta}}{\epsilon_{y,\theta}}$$

where $\epsilon_{y,\theta}$ is the elevated temperature yield strain equal to the elevated temperature 0.2% proof strength $f_{p0.2,\theta}$ divided by the elevated temperature Young's modulus $E_\theta$ (i.e. $\epsilon_{y,\theta} = f_{p0.2,\theta}/E_\theta$), $\sigma$ is the maximum compressive stress and $n_\theta$ is the strain hardening parameter taken from Table 1. As can be seen in Fig. 24, the temperature in the column where the strain limit $\epsilon_{csm,\theta}$ of 0.0022 is attained is equal to 496.13 °C, while the critical temperature $\theta_{cr}$ equal to the temperature at which the axial load in the column returns to its original value $N_{Ed}$ prior to heating is equal to 705.68 °C; thus, the capacity of the column is governed by the strain limit.

*6.2.3. Resistance verification*

The characteristic value of the resistance of the column is equal to the temperature at which the maximum mechanical strain in the critical cross-section first reaches the strain limit. The design value of this resistance $\theta_{Rd}$ is attained by dividing the temperature at which the strain limit is attained $\theta_{csm}$ by the partial factor for resistance in fire conditions $\gamma_{M,fi}$ equal to 1.00 (i.e. $\gamma_{M,fi} = 1.00$), thus the design resistance is given by:

$$\theta_{Rd} = \frac{\theta_{csm}}{\gamma_{M,fi}} = \frac{496.13}{1.00} = 496.13 \text{ °C}$$

Comparing this to the design fire temperature $\theta_{Ed}$ of 450.00 °C:

$$\frac{\theta_{Ed}}{\theta_{Rd}} = \frac{450.00}{496.13} = 0.91 \leq 1.00 \quad \therefore \text{Pass}$$

Therefore, the column is deemed satisfactory.

## 7. Conclusions

In this paper, a new structural steel fire design approach performed by second-order inelastic analysis with strain limits using beam finite elements has been proposed and applied to the fire design of steel columns. Shell finite element models were developed and validated against experimental results performed on steel columns at elevated temperatures using both the isothermal and anisothermal testing approaches. Through the validated shell finite element models, extensive numerical parametric studies were performed to generate structural performance data used in the verification of the proposed fire design

approach. The accuracy of the proposed fire design method was verified considering: (i) various section types, (ii) a range of cross-section and member slenderness values, (iii) major and minor axis column buckling, (iv) axially and rotationally unrestrained, axially restrained and axially and rotationally restrained columns and (v) isothermal and anisothermal analysis techniques. The accuracy and reliability of the proposed fire design method was also compared against those of the simplified calculation model of EN 1993-1-2 [1]. The results of this study demonstrate that the proposed method provides safe-sided design predictions which are consistently more accurate and reliable than the simplified calculation model of EN 1993-1-2 [1]. It should be emphasised that the proposed second-order inelastic analysis with strain limits fire design approach is applied to steel columns as a first step in the establishment of a new fire design approach for steel structures. Future research will extend the proposed method to the fire design of structural systems, including steel frames as well as multi-span steel beams.

**CRediT authorship contribution statement**

**Hasan Murtaza:** Writing – original draft, Visualization, Validation, Software, Methodology, Investigation, Formal analysis, Data curation. **Merih Kucukler:** Writing – review & editing, Writing – original draft, Supervision, Project administration, Methodology, Funding acquisition, Conceptualization.

**Declaration of competing interest**

The authors declare that they have no known competing financial interests or personal relationships that could have appeared to influence the work reported in this paper.

**Data availability**

Data will be made available on request.

**References**

[1] EN 1993-1-2, Eurocode 3 Design of Steel Structures-Part 1-2: General Rules – Structural Fire Design, European Committee for Standardization (CEN), Brussels, 2005.

[2] prEN 1993-1-2, Final Draft of Eurocode 3 Design of Steel Structures-Part 1-2: General Rules – Structural Fire Design, European Committee for Standardization (CEN), Brussels, 2019.

[3] J.M. Franssen, P. Vila Real, Fire Design of Steel Structures, ECCS. John Wiley & Sons, 2016.

[4] T. Von Karman, E.E. Sechler, L.H. Donnell, The strength of thin plates in compression, Trans. Am. Soc. Mech. Eng. 54 (5) (1932) 53–70.

[5] G. Winter, Strength of thin steel compression flanges, Trans. Am. Soc. Civ. Eng. 112 (1) (1947) 527–554.

[6] C. Couto, P. Vila Real, N. Lopes, B. Zhao, Resistance of steel cross-sections with local buckling at elevated temperatures, J. Construct. Steel Res. 109 (2015) 101–114.

[7] C. Couto, P. Vila Real, N. Lopes, B. Zhao, Local buckling in laterally restrained steel beam-columns in case of fire, J. Construct. Steel Res. 122 (2016) 543–556.

[8] É. Maia, C. Couto, P. Vila Real, N. Lopes, Critical temperatures of Class 4 cross-sections, J. Construct. Steel Res. 121 (2016) 370–382.

[9] H. Fang, T.M. Chan, Axial compressive strength of welded S460 steel columns at elevated temperatures, Thin-Walled Struct. 129 (2018) 213–224.

[10] H. Fang, T.M. Chan, Resistance of axially loaded hot-finished S460 and S690 steel square hollow stub columns at elevated temperatures, Structures 17 (2019) 66–73.

[11] C. Maraveas, Local buckling of steel members under fire conditions: A review, Fire Technol. 55 (1) (2019) 51–80.

[12] C. Couto, T. Coderre, P. Vila Real, N. Boissonnade, Cross-section capacity of rhs and shs at elevated temperatures: comparison of design methodologies, Structures 34 (2021) 198–214.

[13] L. Gardner, The continuous strength method, Proc. Inst. Civ. Eng.-Struct. Build. 161 (3) (2008) 127–133.

[14] S. Afshan, L. Gardner, The continuous strength method for structural stainless steel design, Thin-Walled Struct. 68 (2013) 42–49.

[15] A. Fieber, L. Gardner, L. Macorini, Design of structural steel members by advanced inelastic analysis with strain limits, Eng. Struct. 199 (2019) 109624.

[16] A. Fieber, L. Gardner, L. Macorini, Structural steel design using second-order inelastic analysis with strain limits, J. Construct. Steel Res. 168 (2020) 105980.

[17] C. Quan, M. Kucukler, L. Gardner, Design of web-tapered steel I-section members by second-order inelastic analysis with strain limits, Eng. Struct. 224 (2020) 111242.

[18] C. Quan, M. Kucukler, L. Gardner, Out-of-plane stability design of steel beams by second-order inelastic analysis with strain limits, Thin-Walled Struct. 169 (2021) 108352.

[19] F. Walport, L. Gardner, D. Nethercot, Design of structural stainless steel members by second order inelastic analysis with CSM strain limits, Thin-Walled Struct. 159 (2021) 107267.

[20] EN 1993-1-1, Eurocode 3 Design of Steel Structures-Part 1-1: General Rules and Rules for Buildings, European Committee for Standardization (CEN), Brussels, 2005.

[21] EN 1993-1-5, Eurocode 3 Design of Steel Structures-Part 1-5: Plated Structural Elements, European Committee for Standardization (CEN), Brussels, 2005.

[22] L. Gardner, A. Fieber, L. Macorini, Formulae for calculating elastic local buckling stresses of full structural cross-sections, Structures 17 (2019) 2–20.

[23] B.W. Schafer, S. Ádány, Buckling analysis of cold-formed steel members using CUFSM: Conventional and constrained finite strip methods, in: Eighteenth International Specialty Conference on Cold-Formed Steel Structures, 2006, pp. 39–54.

[24] O. Zhao, S. Afshan, L. Gardner, Structural response and continuous strength method design of slender stainless steel cross-sections, Eng. Struct. 140 (2017) 14–25.

[25] M.N. Su, B. Young, L. Gardner, The continuous strength method for the design of aluminium alloy structural elements, Eng. Struct. 122 (2016) 338–348.

[26] A. Liew, L. Gardner, Ultimate capacity of structural steel cross-sections under compression, bending and combined loading, Structures 1 (2015) 2–11.

[27] M. Theofanous, T. Propsert, M. Knobloch, L. Gardner, The continuous strength method for steel cross-section design at elevated temperatures, Thin-Walled Struct. 98 (2016) 94–102.

[28] W. Ramberg, W.R. Osgood, Description of Stress-Strain Curves by Three Parameters, Technical Note No. 902, National Advisory Committee on Aeronautics (NACA), 1943.

[29] E. Mirambell, E. Real, On the calculation of deflections in structural stainless steel beams: An experimental and numerical investigation, J. Construct. Steel Res. 54 (1) (2000) 109–133.

[30] M. Kucukler, Z. Xing, L. Gardner, Behaviour and design of stainless steel I-section columns in fire, J. Construct. Steel Res. 165 (2020) 105890.

[31] M. Kucukler, L. Gardner, L. Macorini, A stiffness reduction method for the in-plane design of structural steel elements, Eng. Struct. 73 (2014) 72–84.

[32] I. González-de-León, I. Arrayago, E. Real, E. Mirambell, A stiffness reduction method for the in-plane design of stainless steel members and frames according with EN 1993-1-4, Eng. Struct. 253 (2022) 113740.

[33] M. Kucukler, L. Gardner, L. Macorini, Development and assessment of a practical stiffness reduction method for the in-plane design of steel frames, J. Construct. Steel Res. 126 (2016) 187–200.

[34] EN 1990-2, Execution of Steel Structures and Aluminium Structures-Part 2: Technical Requirements for Steel Structures, European Committee for Standardization (CEN), Brussels, 2008.

[35] F. Walport, L. Gardner, D. Nethercot, Equivalent bow imperfections for use in design by second order inelastic analysis, Structures 26 (2020) 670–685.

[36] J.M. Franssen, V. Kodur, R. Zaharia, Designing Steel Structures for Fire Safety, CRC Press, 2009.

[37] Abaqus 2018 Reference Manual, Simulia, Dassault Systemes, 2018.

[38] Y.C. Wang, Postbuckling behavior of axially restrained and axially loaded steel columns under fire conditions, J. Struct. Eng. ASCE 130 (3) (2004) 371–380.

[39] ANSYS 18 User Manual, ANSYS Inc, Canonsburg, PA, 2018.

[40] LUSAS Modeller Reference Manual. Version 15.0, LUSAS, Surrey, United Kingdom, 2015.

[41] J.M. Franssen, User's Manual for SAFIR 2011. A Computer Program for Analysis of Structures Subjected to Fire, University of Liege, Belgium, 2011.

[42] M. Kucukler, Lateral instability of steel beams in fire: Behaviour, numerical modelling and design, J. Construct. Steel Res. 170 (2020) 106095.

[43] A. Fieber, L. Gardner, L. Macorini, Formulae for determining elastic local buckling half-wavelengths of structural steel cross-sections, J. Construct. Steel Res. 159 (2019) 493–506.

[44] ECCS, Ultimate Limit State Calculation of Sway Frames with Rigid Joints, Tech. Rep.; No. 33, Technical Committee 8 (TC 8) of European Convention for Constructional Steelwork (ECCS), 1984.

[45] J. Wang, L. Gardner, Flexural buckling of hot-finished high-strength steel RHS and SHS columns, J. Struct. Eng. ASCE 143 (6) (2017) 04017028.

[46] J. Pauli, D. Somaini, M. Knobloch, M. Fontana, Experiments on Steel Columns under Fire Conditions, IBK test report no. 340, Institute of Structural Engineering (IBK), ETH Zürich, 2012.

[47] M.A. Crisfield, A fast incremental/iterative solution procedure that handles "snap-through", Comput. Struct. 13 (1–3) (1981) 55–62.

[48] E. Ramm, Strategies for tracing the nonlinear response near limit points, in: Nonlinear Finite Element Analysis in Structural Mechanics, Springer, 1981, pp. 63–89.

[49] M. Kucukler, Compressive resistance of high-strength and normal-strength steel CHS members at elevated temperatures, Thin-Walled Struct. 152 (2020) 106753.

[50] Z. Xing, M. Kucukler, L. Gardner, Local buckling of stainless steel I-sections in fire: Finite element modelling and design, Thin-Walled Struct. 161 (2021) 107486.

[51] M. Kucukler, Local stability of normal and high strength steel plates at elevated temperatures, Eng. Struct. 243 (2021) 112528.

[52] M. Kucukler, Shear resistance and design of stainless steel plate girders in fire, Eng. Struct. 276 (2023) 115331.

[53] W. Wang, V. Kodur, X. Yang, G. Li, Experimental study on local buckling of axially compressed steel stub columns at elevated temperatures, Thin-Walled Struct. 82 (2014) 33–45.

[54] F. Dumont, E. Wellens, J.-M. Franssen, FIDESC4: Fire Behaviour of Steel Members with Class 4 Cross Sections under Axial Compression with or Without Eccentricity, Report of the experimental tests performed at the University of Liège, 2016.

[55] A.J.P.M. Correia, J.P.C. Rodrigues, Fire resistance of steel columns with restrained thermal elongation, Fire Saf. J. 50 (2012) 1–11.

[56] J. Kruppa, Eurocodes–Fire Parts. Proposal for a Methodology to Check the Accuracy of Assessment Methods, CEN TC250, Horizontal Group Fire, 1999, Document no: 99/130.

[57] J.M. Franssen, Failure temperature of a system comprising a restrained column submitted to fire, Fire Saf. J. 34 (2) (2000) 191–207.

[58] Y. Wang, D. Moore, Effect of thermal restraint on column behaviour in a frame, in: T. Kashiwagi (Ed.), 4th International Symposium on Fire Safety Science, IAFSS, Ottawa, 1994, pp. 1055–1066.

[59] P.G. Shepherd, I. Burgess, On the buckling of axially restrained steel columns in fire, Eng. Struct. 33 (10) (2011) 2832–2838.